

# Euler deconvolution using differential similarity transformations of gravity or magnetic anomalies<sup>1</sup>

Petar Y. Stavrev<sup>2</sup>

## Abstract

Euler deconvolution of gravity and magnetic anomalies can be used to estimate the coordinates of a simple point source and the level of a constant background in the deconvolved field by testing a series of structural indices. By using differential similarity transformations (DSTs), joint estimations of the source coordinates, the structural index and the coefficients of a linear background trend become possible. DSTs, calculated from the derivatives of the interpreted field, depend on the position of a chosen central point of similarity with respect to the source position. On this basis, techniques for Euler deconvolution of anomalous fields are presented.

The theoretical formulations of DST and the deduced sets of equations for Euler deconvolution are tested and verified on model and field examples of magnetic anomalies caused by one-point and two-point sources such as thin and thick dikes, semi-infinite and finite sills, contacts, steps, faulted beds, etc. The possibility of an optimum estimation of the structural index can be used to define a second acceptance criterion along with the criterion of relative standard deviations. The joint application of these two criteria ensures the selection of reliable results. The suggested DST techniques are suitable for initial rapid estimations of the source type, depth and plane location. They may be applied to either profile or gridded data acquired from one-component measurements, as well as from gradient or three-component measurements. Additional data on the density or magnetization of the sources are not necessary.

## Introduction

Euler deconvolution of magnetic and gravity anomalies is based on Euler's homogeneity of the anomalous fields. The degrees of homogeneity  $n$  were first determined for the field strengths of some elementary source models such as a point pole, dipole, sphere, infinite line of poles or dipoles, semi-infinite thin dike, sill, contact, pipe, etc. (Solovev 1960; Hood 1965; Slack, Lynch and Langan 1967; Reid *et al.* 1990). The degree  $n$  with an opposite sign  $N = -n$ , which is called the structural index

---

<sup>1</sup> Paper presented at the 56th EAEG meeting, June 1994, Vienna, Austria. Received July 1994, revision accepted November 1995.

<sup>2</sup> Department of Applied Geophysics, University of Mining & Geology, 1100 Sofia, Bulgaria.

(Thompson 1982), reflects the type of the source and the fall-off rate of its anomaly. The coordinates of a singular point (central, edge, end) of the above-mentioned model sources and the structural index (SI) of their isolated anomalies can be evaluated using a set of Euler's equations for homogeneous functions. Thus, Euler deconvolution (after Reid *et al.* 1990) is implemented as a linear inversion of the anomalous field. Thompson (1982) describes EULDPH, a technique for depth estimates along magnetic profiles assuming a constant background in the deconvolved field. The linear inversion in this case requires  $N$  to be set as a parameter. Estimates of the source shape from magnetic data are reported by Barongo (1984). Euler deconvolution of gridded data in quadratic overlapping windows was confirmed and implemented by Reid *et al.* (1990). Euler deconvolution in three dimensions enables large sets of magnetic and/or gravity data over wide areas to be interpreted rapidly for delineation and depth estimates of different geological structures (Reid *et al.* 1990; Fairhead and Green 1994; Zhaofang Zhu 1994). An important advantage of the method is that depth and shape estimates can be obtained without the need for data on the vector of magnetization or density contrast of the sources. This method, using only simple source approximations, has some limitations regarding its effectiveness, which are discussed in more detail by Reid *et al.* (1990).

Anomalous fields of arbitrarily distributed sources also obey Euler's homogeneity. This property underlies some methods of physical modelling and can be useful in the analytical description, transformation and inversion of anomalous fields (Stavrev 1975). Euler's definition of homogeneous functions, tested on the analytical expressions for gravity or magnetic fields, assumes a geometrical interpretation which leads to the concept of similarity transformations (Stavrev 1981). They result from a similarity space transformation in relation to a given central point and a coefficient of similarity. The differences between the transformed and the original field form differential similarity transformations (DSTs). Their amplitude and distribution depend on the position of the chosen central point of similarity (CPS) with respect to the source position. The inversion techniques described are based on this relationship. This approach can be used to solve the problem for a joint optimum estimation of the structural index and the coordinates of a one-point source and a more complicated two-point source in the presence of a linear background trend. In the case of two-point sources, such as models of thick dikes, finite contacts, sills, pipes, faulted beds, etc., the field inversion based on Euler's homogeneity is a non-linear problem.

The theoretical basis and the respective sets of equations for Euler deconvolution using DST in three- and two-dimensions are given. Model and field examples illustrate the effectiveness of the suggested techniques.

## Theoretical notes

### *Degree of Euler's homogeneity*

According to the Euler's definition, a function  $f(\mathbf{v})$  of a set of variables  $\mathbf{v} = (v_1, v_2, \dots)$

has a degree  $n$ , of homogeneity, if

$$f(t\mathbf{v}) = t^n f(\mathbf{v}), \quad (1)$$

where  $t$  is a real number (see e.g. Apostol 1957). If  $f$  has a differential at  $\mathbf{v}$ , then

$$\mathbf{v} \nabla_{\mathbf{v}} f(\mathbf{v}) = n f(\mathbf{v}). \quad (2)$$

The analytical expressions for gravity or magnetic anomalous fields (see e.g. Telford, Geldart and Sheriff 1990) consist of variables  $\mathbf{v}$  of two main types: coordinates of the observation points and quantities describing the field sources. The sources are masses or dipoles (equivalent magnetic sources) distributed discretely or continuously in geometrical objects (figures) in the space. Their description involves two kinds of quantity: geometrical and physical. These are called the source parameters and are either fixed in a direct problem or variable in an inverse modelling. The shape, size and position of the source figures are determined by geometrical parameters, which either can have dimensions, i.e. length measurements such as coordinates, thickness, radius, area, volume or can be dimensionless quantities such as the ratio of lengths, angles. The real source figures are finite solids with arbitrary shapes. In the theory, source distributions in semi-infinite solids and volumeless figures (point, line, surface) serve as useful approximations or as equivalent representations of the real sources and their fields. Thus, the basic types of source figure are point, line (straight or curved), surface and solid objects classified by the number  $d$  of their dimensions being 0, 1, 2 and 3, respectively. The quantity and the distribution of point masses or dipoles in the figures are determined by scalar and vector physical parameters, i.e. quantities of point masses or dipole moments and line, surface and volume densities of point masses or dipole moments in the corresponding figures. An adequate 'geometrical' type of the physical parameters can be specified by an index  $u$ , so that  $u = 0$  for the quantities of point masses or moments and  $u = 1, 2$  and  $3$  for the line, surface and volume densities of point masses or moments, respectively. Another index  $s$  for the type of gravity and magnetic source will be used, so that  $s = 1$  for point masses and equivalent poles,  $s = 2$  for dipoles,  $s = 3$  for equivalent quadrupoles.

For the following analysis of Euler's homogeneity the well-known analytical expressions for the additive elements of anomalous fields caused by simple interpretation models (e.g. Telford *et al.* 1990) can be represented in the form

$$A_{s,k} = \beta m_u f_g(x - x_{01}, y - y_{01}, z - z_{01}, \dots, x - x_{0q}, y - y_{0q}, z - z_{0q}, \mathbf{h}, \boldsymbol{\phi}), \quad (3)$$

where  $A$  is a potential or each of its derivatives of order  $k$ ,  $k = 0, 1, 2, \dots, s$  and  $u$  are the above-defined indices,  $\beta$  is a constant,  $m_u$  is a constant physical parameter of type  $u$ ,  $f_g$  is a function of geometrical variables, containing components of the distance vectors between an observation point  $P(x, y, z)$  and the points  $M_j(x_{0j}, y_{0j}, z_{0j})$ ,  $j = 1, 2, \dots, q$ , which describe the source figure. The expression may or may not include a set  $\mathbf{h}$  of dimensional geometrical parameters and a set  $\boldsymbol{\phi}$  of dimensionless parameters of the figure and angles of orientation of a vector physical parameter. For example, in the

expression for the vertical gravity field strength  $g$  caused by a finite dipping thin sheet,

$$g = \gamma \rho h \{ \sin \alpha \ln(r_2/r_1)^2 - 2(\theta_1 + \theta_2) \cos \alpha \}, \quad (4)$$

the field  $g$  has indices  $s = 1$  for the type of source (point masses) and  $k = 1$  for the first vertical derivative,  $g = \partial V / \partial z$ , of the gravity potential  $V$ , i.e.  $g = A_{1,1}$ ;  $\gamma$  is the gravitational constant;  $\rho$  is the volume density ( $u = 3$ ) of point masses, i.e.  $\rho = m_3$ ; the multiplier  $h\{\cdot\}$  is the geometrical function  $f_g$ , which includes the thickness  $h$  of the sheet, the distances  $r_1$  and  $r_2$  between the observation points  $P$  and the two edge points  $M_1$  and  $M_2$  of the sheet, the angle  $(\theta_1 + \theta_2)$  of 'seeing' the sheet from point  $P$ , and the dip angle  $\alpha$ .

Testing Euler's definition (1) on the analytical expressions (3) for gravity and magnetic anomalies and their derivatives leads to the following main results.

(a) As a rule, the elements  $A_{s,k}$  are not homogeneous functions of the set of variables consisting only of the coordinates of the observation points  $P$ . An exception exists in the case of one point source ( $q = 1$  in (3)), when the origin of the coordinates coincides with the singular source point  $M$ .

(b) Expressions (3) are homogeneous functions in relation to a set of variables consisting of all dimensional geometrical quantities, i.e. the coordinates of the observation points and the respective geometrical parameters of the source. The angular geometrical parameters are not variables of homogeneity. The degree of homogeneity  $n$  decreases with increasing order  $k$  of the field elements as derivatives of the respective potential. For a given order  $k$  and a given figure of the causative body, the degree  $n$  of the respective magnetic anomaly is one less than the degree  $n$  of the gravity anomaly. The value of  $n$  can be represented by the following formula

$$n = u - s - k, \quad (5)$$

where  $u$ ,  $s$  and  $k$  are integers defined in (3). The value of  $n$  is equal to the power of the unit (metre, foot) of the function  $f_g$  in (3). In (4),  $n = 3 - 1 - 1 = 1$ .

If the physical parameter in (3) is of the type  $u = d$ , then

$$n = d - s - k, \quad (6)$$

where  $d$  is the number of dimensions of the source figure, and  $d = 0, 1, 2$  or  $3$ . The physical parameters with a different index  $u$  are contained in the relationship  $m_u = c m_d h_w$ , where  $c$  is a constant,  $h_w$  consists of one, two or three sizes and has a unit to the power  $w = d - u$ . For example, in (4),  $\rho$  has  $u = 3$ , while the source figure is approximated to a plane having  $d = 2$  and surface density  $\sigma = \rho h$ , or  $\rho = \sigma h^{-1}$ , i.e.  $w = 2 - 3 = -1$ . Substitution of  $\rho h$  by  $\sigma$  in (4) reduces the degree of homogeneity of  $g$  by one, i.e.  $n = 2 - 1 - 1 = 0$ .

(c) The physical parameter in (3) can be treated as a variable of homogeneity, either individually or together with the dimensional geometrical variables. If the physical parameter is a vector, then its angles of orientation are not variables of homogeneity. The degree  $n$  of  $A_{s,k}$  in relation to  $m_u$  is equal to one.

In the complicated case of an anomalous field caused by a set of individual sources,

the additive elements of the field are homogeneous functions of all dimensional geometrical variables if the physical parameters of all sources can be represented by an equal index  $u$ . Obviously, this unification is possible for a set of sources with the same dimension  $d$ , because  $u = d$ , independently of the number, shape and size of the single sources. Thus, Euler's homogeneity is valid for the field of a set of sources with figures of equal dimension  $d$ . In the case of different  $d$  in a set of finite source figures, the unification of  $u$  is always possible for  $u = 0$ , i.e. for the entire mass or magnetic moment of each source. It means that the degree  $n_{\min} = -s - k$  (see (5)) is an inherent degree for the real fields of finite causative bodies. In the 2D theoretical approximation of sources to an infinite horizontal extent, the required unification of  $u$  is possible for  $u = 1$  (mass or moment per unit length), if the cross-sections of all causative bodies are finite. Thus, the corresponding minimum degree is  $n_{\min} = 1 - s - k$ . In the case of semi-infinite theoretical source approximations in 3D and 2D problems, the minimum degree of homogeneity for the determinable elements of the field is  $n_{\min} = d - s - k$ . In all cases the maximum possible degree is  $n_{\max} = 3 - s - k$ . Therefore, the range of the degree  $n$  of Euler's homogeneity of gravity ( $s = 1$ ) and magnetic ( $s = 2$ ) anomalies is

$$(3 - s - k) - D \leq n \leq (3 - s - k), \quad (7)$$

where  $D = 3$  in 3D problems and  $D = 2$  in 2D problems.

Euler's homogeneity in relation to all dimensional geometrical variables is of interest in the gravity and magnetic inverse problems. The degree of homogeneity of a given anomaly may not be unique (see (5)). This fact is explained after geometrical and physical interpretation of Euler's definition (1).

#### Similarity transformations

Consider a gravity or magnetic anomaly  $A$  as a homogeneous function of variables  $\mathbf{v}$ , which include the coordinates of observation points  $P$  and all dimensional geometrical parameters of the figure  $B$  of a source with a physical parameter  $m_u$ , in a Cartesian coordinate system  $XYZ$ . In the left-hand side of Euler's definition (1), each variable  $v_j$ ,  $j = 1, 2, \dots$ , has to be multiplied by a real number  $t$ . This means that points  $P(x, y, z)$  shift to points  $P'(x', y', z')$ , where  $x' = tx$ ,  $y' = ty$ ,  $z' = tz$ , and points  $M(x_0, y_0, z_0)$  of the figure  $B$ , shift to points  $M'(x'_0, y'_0, z'_0)$ , where  $x'_0 = tx_0$ ,  $y'_0 = ty_0$ ,  $z'_0 = tz_0$ , thus forming a figure  $B'$ . The physical parameter  $m_u$  is not considered a variable of homogeneity, so it preserves its type and value in  $B'$ . Thus, the left hand side of (1) for an anomaly  $A$  can be treated as an anomaly  $A(P')$  caused by the shifted source in the shifted observation points  $P'$ . Hence, an equivalent form of (1) for homogeneous anomalies  $A$  is

$$A(P'; B', m_u) = t^n A(P; B, m_u), \quad (8)$$

where the degree of homogeneity  $n$  is determined by (5).

The multiplication of all dimensional geometrical variables of  $A$  by a real number  $t \neq 0$  generates a homotopic geometrical transformation (e.g. Fishback 1964) with a

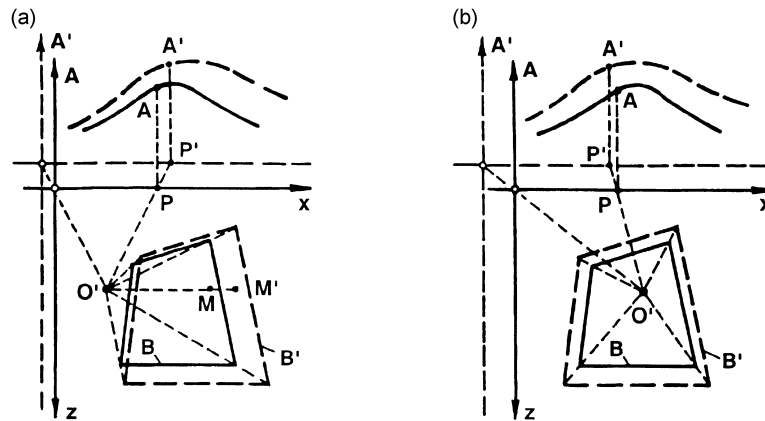
central point at the origin  $O$  of the coordinates (see (B4) in Appendix B). In relation to another centre  $O'(a, b, c)$ , the respective transformation is

$$x' = tx + (1 - t)a, \quad y' = ty + (1 - t)b, \quad z' = tz + (1 - t)c, \quad x'_0 = tx_0 + (1 - t)a, \dots \quad (9)$$

For  $t > 0$ , these equations define a similarity transformation (see (B3)) which preserves the parallelism or the angle between two lines, the ratio of two segments, the integrity, shape and orientation of the geometrical figures (Fig. 1). The lengths, areas and volumes are changed by a factor  $t^d$ ,  $d = 1, 2$  and  $3$ , respectively.

Equations (8) and (9) determine a direct similarity transformation of an anomaly  $A(P)$  into a calculable anomaly  $A(P')$  in relation to a given central point of similarity (CPS)  $O'(a, b, c)$  and a given coefficient of similarity  $t > 0$ . This transformation does not concern angular quantities of the figures and of the vector physical parameters. As a result these quantities are not variables of Euler's homogeneity. The value of the accepted physical parameter does not undergo any change, but other possible parameters undergo changes due to the changes in the figure sizes. For example, if the volume density  $\rho$  ( $u = 3$ ) of point masses  $m$  preserves its value in the transformed solid  $B'$  ( $d = 3$ ), then the complete mass in  $B'$  is  $m' = t^3 m$ , and if  $m$  ( $u = 0$ ) preserves its value in  $B'$ , then  $\rho' = t^{-3} \rho$ . The respective anomalies  $A(P')$  in these two different cases are related by the coefficient  $t^3$ . This means that two degrees of homogeneity differing by 3 are possible for the original anomaly  $A(P)$ . The choice of different indices  $u$  or degrees  $n$  (see (5)), corresponds to different quantities and distributions of point masses or dipoles in  $B'$ .

For solving gravity and magnetic inverse problems, useful relationships on the basis



**Figure 1.** Similarity 2D transformations of the causative body  $B$  into  $B'$  and the respective transformations of its anomaly  $A$  into  $A' = A(P')$  in relation to a central point of similarity  $O'$  (a) outside and (b) inside the body  $B$ .

of similarity transformations (8) can be obtained by considering the differences  $D$  between the transformed anomalies and the original anomaly,

$$D(P') = A(P'; B', m_u) - A(P'; B, m_u), \quad (10)$$

where  $A(P'; B', m_u)$  is defined by  $A(P; B, m_u)$  from (8),  $A(P'; B, m_u)$  can be measured or is the analytically continued original anomaly  $A$  in the transformed observation points  $P'$ .  $D(P')$  depends on the choice of  $O'(a, b, c)$ ,  $n$  and  $t$ . Elimination of the dependence on  $t$  is possible for the derivative  $S$  of  $D$  at  $t$ , when  $t$  tends to unity. According to (8), (9) and (10),  $S(P') = dD(P')/dt = n t^{n-1} A(P; B, m_u) - \mathbf{R}_{O'P} \nabla_{P'} A(P'; B, m_u)$ . If  $t$  tends to 1, then  $P'$  tends to  $P$  and the last equation results in

$$S(P) = nA(P) - \mathbf{R}_{O'P} \nabla_P A(P), \quad (11)$$

where  $\mathbf{R}_{O'P}$  is a vector from a point  $O'$  to the point  $P$ ,  $\mathbf{R}_{O'P} = \mathbf{R}_{OP} - \mathbf{R}_{OO'}$ . This is a differential similarity transformation (DST) determined for observation points  $P$  of the original anomaly  $A$ . DST depends on two parameters, the degree  $n$  (or index  $u$ , see (5)) and the radius-vector  $\mathbf{R}_{OO'}$  of CPS  $O'(a, b, c)$ . Using (11) a parametrical operator  $S[A]$ , applied to a differentiable function  $A(x, y, z)$ , is defined. With appropriate indices, the analytical expression of DST (11) in Cartesian coordinates is

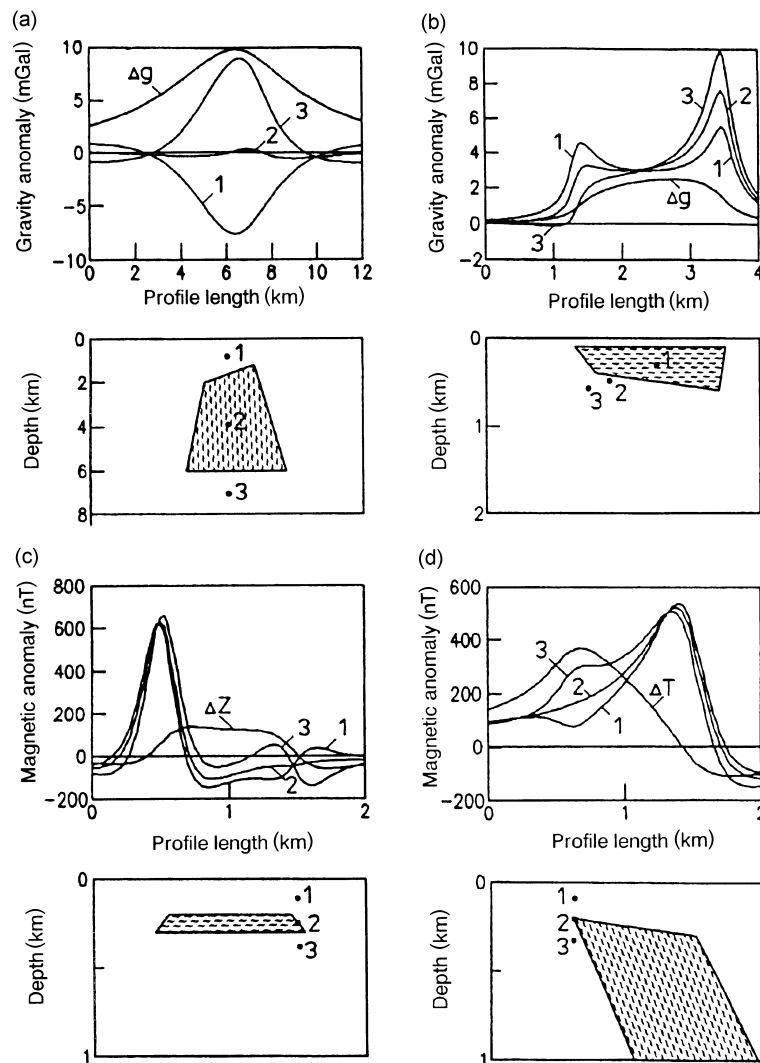
$$S_u^{(n)}[A_{s,k}(x, y, z)]_{(a,b,c)} = (u - s - k)A - (x - a)\partial A/\partial x - (y - b)\partial A/\partial y - (z - c)\partial A/\partial z, \quad (12)$$

where  $u$ ,  $s$  and  $k$  are determined in (3). The indices of  $S[A]$  will be used according to the dependent parameters under consideration. The following formal properties of  $S[A]$  proceed from (12):

$$\begin{aligned} S_u[\beta A_1 + \eta A_2] &= \beta S_u[A_1] + \eta S_u[A_2], \\ S_{u_2}[A] &= S_{u_1}[A] + (u_2 - u_1)A, \\ S[A]_{O'_2} &= S[A]_{O'_1} + \mathbf{R}_{O'_1 O'_2} \nabla_P A, \\ S[\partial A/\partial v] &= \partial S[A]/\partial v, \end{aligned} \quad (13)$$

where  $\beta$ ,  $\eta$  are two numbers,  $A_1$  and  $A_2$  are two additive anomalies,  $u_1$ ,  $u_2$  and  $O'_1$ ,  $O'_2$  are two different parameters  $u$  and CPS  $O'$ ,  $v$  is the  $x$ -,  $y$ - or  $z$ -coordinate of point  $P$ .

The usefulness of DST in gravity and magnetic Euler inversions becomes apparent after treating their properties as calculable anomalies of equivalent sources (see Appendix A). The distribution and amplitude of  $S_u[A(x, y, z)]_{O'}$  are closely related to the position of  $O'(a, b, c)$  with respect to the source of  $A$ . For example, the coincidence of a chosen point  $O'$  with a point dipole at point  $M$  reduces  $S[A]_M$  to a value of zero at all observation points. In this and in more complicated cases, the characteristics of  $S[A]$  reflect the shape, depth and location of the source. Model curves of  $S[A]$  transformations of 2D gravity and magnetic anomalies are shown in Fig. 2.



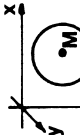
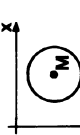

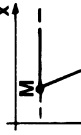

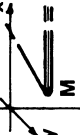



**Figure 2.** Model curves of 2D differential similarity transformations: (a)  $S_1[\Delta g]$ , (b)  $S_3[\Delta g]$ , (c)  $S_2[\Delta Z]$ , (d)  $S_3[\Delta T]$ . The curve's number corresponds to the number of the central point of similarity  $O'$  shown by a bold point on the vertical cross-section of the causative body.

#### *Euler deconvolution of anomalies caused by one-point sources*

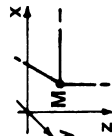
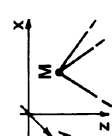
Euler deconvolution (Reid *et al.* 1990) is based on Euler's equation (2), applied to measured magnetic and gravity anomalies on the assumption of proximity to the anomalous fields of point sources (Thompson 1982). This type of source will be denoted here as a one-point source. The theoretical models of one-point sources are shown in Table 1. The upper part of Table 1 consists of well-known models used mainly in the magnetic interpretation. In the lower part some possible 3D models are



Table 1. Structural indices  $N$  of gravity and magnetic anomalies of one-point sources.

One-point source				Anomaly			
Name	Figure	Dimension		Type $s$	Gravity, Magnetic field		
		$d$			Dimension $D$	Potential $k = 0$	Gradients $k = 2$
Point mass, sphere		0		1	3	1	3
Point dipole, sphere		0		2	3	2	4
Line of masses, circular cylinder		1		1	2	0	2
Line of dipoles, circular cylinder		1		2	2	1	3
Semi-infinite plane,		2		1	2	-1	1
thin dike, sill, step, bed		2		2	2	0	2
Semi-infinite contact		3		1	2	-2	0
		3		2	2	-1	1
Semi-infinite line of masses or dipoles,		1		1	3	0	2
thin rod, pipe		1		2	3	1	3
Semi-infinite triangular plane, thin plate		2		1	3	-1	1
		2		2	3	0	2

**Table 1.** Continued

One-point source				Anomaly					
Name	Figure	Dimension $d$	Type $s$	Dimension $D$	Gravity, Magnetic field			Structural index $N$	
					Potential $k = 0$	Strengths $k = 1$	Gradients $k = 2$		
Semi-infinite parallelepiped block		3	1	3	G	-2	-1	0	
		3	2	3	M	-1	0	1	
Semi-infinite pyramid, cone		3	1	3	G	-2	-1	0	
		3	2	3	M	-1	0	1	

given. The solid models of a sphere, circular cylinder, thin pipe, sill, dike, step or plate are equivalent or close to the corresponding volumeless theoretical models of a point, line or plane. The geometrical description of all one-point sources includes the coordinates of one singular point  $M(x_0, y_0, z_0)$ , the central, edge, vertex point of the figure, and a set of possible angular quantities in the case of a semi-infinite figure. The density of point masses or dipoles is a constant. According to (3), a common analytical expression for the determinable elements  $A_{s,k}$  of anomalous fields, caused by one-point sources, is

$$A_{s,k} = \beta m_d f_g(x - x_0, y - y_0, z - z_0, \phi), \quad (14)$$

where  $d$  is the dimension of the theoretical one-point source figure. The equivalent solid models have the same expression for  $A_{s,k}$  if the type  $u$  of their physical parameters is chosen to be equal to the dimension  $d$  of the respective theoretical model. This condition involves the size (radius or thickness) of the solid figure in the expression for  $m_d$  (see (4)). Thus, the dimensional geometrical parameters of a one-point source are represented by the coordinates of one point only. This fact can be used as a definition of the term ‘one-point source’. The degree of homogeneity  $n$  of  $A_{s,k}$  (14) has a unique value, according to (6).

Euler’s equation (2) for an anomalous field  $A$  of type (14) is

$$\mathbf{R}_{OP} \nabla_P A + \mathbf{R}_{OM} \nabla_M A = nA, \quad (15)$$

where  $\mathbf{R}_{OP}$  and  $\mathbf{R}_{OM}$  are radius-vectors of the points  $P$  and  $M$ , respectively. According to (14),  $\nabla_M A = -\nabla_P A$ . This equation makes it possible for the unknown gradient  $\nabla_M A$  to be substituted by the gradient  $\nabla_P A$  whose components can be found from measurements or calculations. Thus, in Cartesian coordinates, (15) takes the form

$$x_0 \partial A / \partial x + y_0 \partial A / \partial y + z_0 \partial A / \partial z + nA = x \partial A / \partial x + y \partial A / \partial y + z \partial A / \partial z. \quad (16)$$

The Euler deconvolution of  $A$  is based on the solution of an overdetermined set of linear equations (16) in relation to the unknowns  $x_0, y_0, z_0, n$ .

Thompson (1982) refers to  $(-n) = N$  as a structural index (SI). According to (6), the formula for  $N$  is

$$N = s + k - d, \quad (17)$$

where  $d$  corresponds to the theoretical one-point sources. The SI of the gravity and magnetic potentials, strength (and magnetic induction) components and their gradients caused by one-point sources, are given in Table 1. All known indices (Thompson 1982; Reid *et al.* 1990) are in accordance with those shown in Table 1. The value of  $N$ , depending on the dimension  $d$  (see (17)), reflects the type of the causative one-point source. The corresponding anomaly has a fall-off rate proportional to  $1/r^N$  (Thompson 1982). This relationship has to be considered along radial lines  $r(\theta, \psi)$  originating from the singular point  $M$  of the source. According to (8) and (14), in spherical coordinates  $(r, \theta, \psi)$ ,

$$A_{s,k}(r, \theta, \psi; \phi) = A_{s,k}(r_0, \theta, \psi; \phi)(r_0/r)^N,$$

where  $r_0$  is a constant distance. The positive values of  $N$  correspond to the natural attenuation of  $A_{s,k}$  with the distance  $r$ . If  $N = 0$ , then  $A_{s,k}$  is a constant, depending on the orientation of  $r(\theta, \psi)$ . This is possible for some anomalies such as 2D gravity  $g$  of a thin step, while  $g$  of a semi-infinite dipping dike is not determinable. The indeterminable elements  $A_{s,k}$  of some semi-infinite one-point sources have  $(s + k) < d$  and negative  $N$  (Table 1). The real sources are finite and all elements  $A_{s,k}$  of their outer fields are determinable, independently of the sign of the degree  $n$  of Euler's homogeneity. A real source, such as a thin dike or a finite step with comparatively large but limited depth extent, is not a one-point source because of the existence of two singular source points. When  $n < 0$  ( $N > 0$ ) the effect of this second point is negligible. In the case  $n > 0$  ( $N < 0$ ) the effect of a source limitation is equivalent to an occurrence of a linear background trend in the deconvolved anomaly (see (A9)). The effect is non-linear if the size of a real source is commensurable with its depth.

The observed gravity and magnetic fields  $F$  consist of systematic and random noise. Thompson (1982) derived the equation for Euler deconvolution of 2D magnetic anomalies in the presence of a constant background  $B_0$ . In 2D and 3D gravity and magnetic problems, if  $F = A + B_0$ , then putting  $A = F - B_0$  in (15) yields

$$\mathbf{R}_{OM} \nabla_P F(P) + NB_0 - NF(P) = \mathbf{R}_{OP} \nabla_P F(P). \quad (18)$$

The linearity of (18) in relation to the full list of unknowns  $(x_0, y_0, z_0, N, B_0)$  is perturbed by the term  $NB_0$ . By using a series of prescribed  $N$ , Thompson (1982) in a 2D deconvolution and Reid *et al.* (1990) in a 3D deconvolution were able to preserve the linearity of (18). The correct  $N$  among the prescribed values corresponds to the best acceptable quality of the least-squares estimations of the other unknowns.

A linear change in the background of a local anomaly  $A$  occurs very often, due to a regional field and peripheral fields of side sources. They create additional complications in the respective form of Euler's equation. Consider a linear background field

$$\Phi(P) = B_0 + b_x x + b_y y + b_z z = B_0 + \mathbf{b} \mathbf{R}_{OP}. \quad (19)$$

According to (15) for  $A = F - \Phi$ ,

$$\mathbf{R}_{OM} \nabla_P F(P) + NB_0 - NF(P) + \{(N + 1)\mathbf{R}_{OP} - \mathbf{R}_{OM}\} \mathbf{b} = \mathbf{R}_{OP} \nabla_P F(P). \quad (20)$$

The term  $\{\cdot\} \mathbf{b}$  is a supplement to the left-hand side of (18). This term consists of unknown vectors  $\mathbf{R}_{OM}$  and  $\mathbf{b}$  in a non-linear relationship. If the gradient  $\mathbf{b}$  is significant, then some deviations in the results of the deconvolution, based on (18), may occur.

A non-linear side component in a deconvolved anomaly can be approximated to a field of another one-point source, which is close to the main one-point source. If  $F = A_1 + A_2$ , where  $A_1$  and  $A_2$  are elements of the field of two one-point sources with an equal dimension  $d$  and singular points  $M_1$  and  $M_2$ , then Euler's equation (2) takes the form

$$\mathbf{R}_{OM_1} \nabla_{M_1} F + \mathbf{R}_{OM_2} \nabla_{M_2} F + NF = -\mathbf{R}_{OP} \nabla_P F, \quad (21)$$

where  $\nabla_{M_1}F = \nabla_{M_1}A_1 = -\nabla_P A_1$ ,  $\nabla_{M_2}F = \nabla_{M_2}A_2 = -\nabla_P A_2$ , and therefore

$$\nabla_{M_1}F + \nabla_{M_2}F = -\nabla_P F. \quad (22)$$

This relationship does not allow substitution of the unknown gradients  $\nabla_{M_1}F$  and  $\nabla_{M_2}F$  by the measurable or calculable gradient  $\nabla_P F$ . It means that (21) cannot be reduced to a linear equation in relation to the unknown coordinates of  $M_1$  and  $M_2$ .

The above-mentioned difficulties in solving Euler's equations in the presence of a linear background trend and non-linear interference in a deconvolved anomalous field can be overcome by using differential similarity transformations of the observed field.

### Euler deconvolution using differential similarity transformations

#### One-point source anomalies

Consider an anomalous field  $A$  of a one-point source given by (14) in the presence of a background trend  $\Phi$  given by (19), i.e. the observed field is  $F = A + \Phi$ . The operator of DST (12), applied to the field  $A = F - \Phi$  having structural index  $N$  given by (17), yields at each observation point  $P$

$$S^{(-N)}[A]_{O'} = S^{(-N)}[F]_{O'} - S^{(-N)}[\Phi]_{O'}, \quad (23)$$

$$\text{where } S^{(-N)}[F]_{O'} = -NF(P) - \mathbf{R}_{O'P}\nabla_P F(P), \quad (24)$$

$$S^{(-N)}[\Phi]_{O'} = -N\Phi(P) - \mathbf{R}_{O'P}\nabla_P \Phi(P) = -NB_0 - \{N\mathbf{R}_{OP} + \mathbf{R}_{O'P}\}\mathbf{b}. \quad (25)$$

Euler's equation (15), after adding a term  $\{-\mathbf{R}_{OO'}\nabla_P A\}$  to its two sides and taking into account (23)–(25), can be expressed as

$$\mathbf{R}_{O'M}\nabla_P F + NB_0 + \{N\mathbf{R}_{OP} + \mathbf{R}_{O'P} - \mathbf{R}_{O'M}\}\mathbf{b} = -S^{(-N)}[F]_{O'}. \quad (26)$$

The right-hand side of (26) can be calculated using (24). The left-hand side contains the unknowns  $\mathbf{R}_{O'M}$ ,  $N$ ,  $B_0$  and  $\mathbf{b}$  in a non-linear relationship. If a CPS  $O'(a, b, c)$  coincides with the singular point  $M(x_0, y_0, z_0)$  of the source, then  $\mathbf{R}_{O'M} = 0$  and from (26) it follows that

$$NB_0 + \{N\mathbf{R}_{OP} + \mathbf{R}_{MP}\}\mathbf{b} = -S^{(-N)}[F]_M. \quad (27)$$

Obviously, in this case the S-transformation turns into a linear function of the coordinates of observation points  $P(x, y, z)$ , thus coinciding with the S-transformation of the linear background  $\Phi$  given by (25). Therefore, according to (23),

$$S^{(-N)}[A]_M = 0. \quad (28)$$

This formal result is verified by the physical interpretation of DST (see Appendix A).

If the structural index is not correctly prescribed in (26), then according to (27),

$$(N_1 - \Delta N)B_0 + \{(N_1 - \Delta N)\mathbf{R}_{OP} + \mathbf{R}_{MP}\}\mathbf{b} + \Delta NF(P) = -S^{(-N)}[F]_M,$$

where  $N_1$  is the incorrect index differing by  $\Delta N$  from the correct index  $N$ . This

transformation is not a linear function because of the non-linear term  $\Delta N F(P)$ . Therefore, only the correct index  $N$  allows linearization of  $S[F]_M$ . If  $O' = M$ , then the coefficients of the background trend  $\Phi$  can be estimated from (27).

The possibilities described for determination of the unknowns in (26) lead to a method of Euler deconvolution based on the linearization of DST by selection of an appropriate CPS. A quantitative indication of the linearity of DST is the residual dispersion  $Q^2[S]$  of  $S(P)$  about its linear regression on a set of observation points (see e.g. Draper and Smith 1966), i.e.

$$Q^2[S] = \Sigma \{S(P_i) - q_0 - \mathbf{q}\mathbf{R}_{OP_i}\}^2 / (K - U_c), \quad i = 1, 2, \dots, K, \quad (29)$$

where  $S(P_i) = S^{(-N)}[F(P_i)]_{O'}$  (see (24)),  $q_0$  and the components  $q_x, q_y, q_z$  of the vector  $\mathbf{q}$  are regression coefficients,  $U_c$  is the number of coefficients and  $K$  is the number of observation points  $P_i(x_i, y_i, z_i)$  involved in the regression. For a linear function  $S(P)$  the value of  $Q$  is equal to zero. In the presence of noise in the observed field  $F$  and its gradient  $\nabla_P F$ , the minimum of  $Q^2$  should be found by selecting the parameters  $a, b, c$  and  $N$  of  $S[F]$ , i.e. the least-squares problem,

$$Q^2(a, b, c, N) = \min, \quad (30)$$

should be solved. The condition (30), treated in a square window on a map of gridded data, leads to the system of normal equations

$$\Sigma t_{ij} p_j = r_i, \quad i = 1, 2, 3, 4, \quad j = 1, 2, 3, 4, \quad (31)$$

where  $p_1 = a, p_2 = b, p_3 = c, p_4 = -N$ ,

$$t_{ij} = \Sigma \{E_m[D_j]E_m[D_i]\}, \quad m = 1, 2, \dots, K,$$

$$r_i = \Sigma \{G_m E_m[D_i]\}, \quad G_m = E_m[xD_1] + E_m[yD_2] + E_m[zD_3],$$

$$D_1 = \partial F / \partial x, \quad D_2 = \partial F / \partial y, \quad D_3 = \partial F / \partial z, \quad D_4 = F,$$

$$E_m[H] = H_m - H_0 - \mathbf{q}[H]\mathbf{R}_{O_c P}, \quad H_m = H(x_m, y_m, z_m),$$

$$H_0 = \Sigma H_w / K, \quad q_v[H] = \Sigma \{(v_w - v_c)(H_w - H_0)\} / \Sigma (v_w - v_c)^2, \quad w = 1, 2, \dots, K,$$

where  $v = x, y$  or  $z$ , i.e. coordinates of the observation points  $P$ ,

$v_c = x_c, y_c$  or  $z_c$ , i.e. coordinates of the window central point  $O_c$ ,

and  $H$  is a common symbol of the functions on which the operator  $E$  is exercised.

The solution of (31) gives optimal values of the coordinates  $x_0, y_0, z_0$  of the singular point  $M$ , the structural index  $N$  and the coefficients of the background trend  $\Phi$ :

$$x_0 = p_1, \quad y_0 = p_2, \quad z_0 = p_3, \quad N = -p_4, \quad (32)$$

$$b_v = q_v / (p_4 - 1), \quad v = x, y \text{ or } z, \quad (33)$$

$$B_0(x_c, y_c, z_c) = \{S_0 - (p_1 - x_c)b_x - (p_2 - y_c)b_y - (p_3 - z_c)b_z\} / p_4, \quad (34)$$

where  $q_v = \Sigma\{(v_m - v_c)(S_m - S_0)\} / \Sigma(v_m - v_c)^2$ ,  $m = 1, 2, \dots, K$ ,

$$S_m = p_4 F_m - (x_m - p_1)(D_1)_m - (y_m - p_2)(D_2)_m - (z_m - p_3)(D_3)_m,$$

$$S_0 = \Sigma S_w / K, \quad w = 1, 2, \dots, K.$$

The quality of solutions obtained in this way is estimated by the minimum  $Q_m^2$  of the object function  $Q^2[S]$ . According to (31)–(34)

$$Q_m^2 = \Sigma\{S_m - S_0 - (x_m - x_c)q_x - (y_m - y_c)q_y - (z_m - z_c)q_z\}^2 / (K - U_c),$$

$$m = 1, 2, \dots, K. \quad (35)$$

The dispersions  $\sigma^2$  of the solutions of system (31) are determined by the formulae

$$\sigma_i^2 = d_{ii} Q_m^2 (K - U_c) / (K - U), \quad i = 1, 2, 3, 4, \quad (36)$$

where  $d_{ii}$  are the diagonal elements of the inverse matrix of the coefficients  $t_{ij}$  in (31),  $U$  is the number of unknowns ( $U = 4$ ),  $K$  is the number of points in the window.

In (29)–(35), it is assumed that the field  $F$  and components  $D_1, D_2, D_3$  of its gradient are known on a inclined surface of observation. If in a given window this surface is a horizontal plane, then the vertical gradient  $b_z$  of the background is indeterminable (see (33)). According to the same equation, the total gradient  $\mathbf{b}$  is indeterminable if  $p_4 = 1$ , i.e.  $N = -1$ . The coefficient  $B_0$  cannot be determined when  $p_4 = 0$ , i.e. when  $N = 0$ . In this case  $S^{(0)}[F]$  does not depend on the coefficient  $B_0$  (see (25)).

For the profile deconvolution of a 2D anomaly in the plane  $XOZ$ , the normal system of equations is derived from system (31) after excluding the second row and second column and removing all quantities related to the direction of the  $y$ -axis in (29)–(36). Thus, a  $3 \times 3$  system of the unknowns  $a, c, N$  ( $U = 3$ ) has to be solved in windows along the profile.

The system (31) has a unique solution if  $F(P)$  is not a linear or quadratic function within the window. If a 2D field occurs in the square window, then the solution of the problem as a 3D problem will cause deterioration of the solution quality, especially regarding the horizontal coordinates of the source. To solve the problem as a 2D problem, it is necessary to determine the orientation of the horizontal gradient of anomaly  $A(P)$  of the source in the presence of a linear background trend  $\Phi(P)$  and random noise. The projection of the horizontal gradient of  $F(P)$  has minimum variations in the direction perpendicular to the horizontal gradient of  $A$ . For a preset direction  $X'$  at an angle  $\psi$  to the  $X$ -axis, the projection of  $\nabla_P F$  is

$$D_{1,2}(P) = D_1(P) \cos \psi + D_2(P) \sin \psi. \quad (37)$$

The extremum problem is

$$Q^2(\psi) = \Sigma\{E_m[D_{1,2}]\}^2 = \min, \quad m = 1, 2, \dots, K, \quad (38)$$

whose solution is

$$\psi_1 = \tan^{-1}\{2t_{12}/(t_{11} - t_{22})\}/2 \text{ or } \psi_2 = \psi_1 + \pi/2, \quad (39)$$

where the coefficients  $t_{11}$ ,  $t_{12}$  and  $t_{22}$  are determined in (31). The angle  $\psi_0$ , which indicates the orientation  $X'$  of the gradient of the 2D field  $A$ , is either angle  $\psi_1$  or angle  $\psi_2$  depending on which gives the greater value of  $Q^2(\psi)$ . The condition for non-two-dimensionality of the field in the window is

$$Q^2(\psi_0 + \pi/2) > p\varepsilon^2, \quad (40)$$

where  $\varepsilon^2$  is the noise dispersion in the derivatives  $D_1$  and  $D_2$ ,  $p > 1$  is a coefficient chosen according to the desired degree of approximation. If condition (40) is not satisfied, then the deconvolution can be carried out as 2D along line  $X'$  passing through the window centre  $O_c(x_c, y_c, z_c)$  at an angle of  $\psi_0$  to the  $X$ -axis. All data in the window points can be involved using projections (37) along the  $X'$ -axis.

The presence of random noise in the data increases the dispersions (36) of the results. A preliminary noise suppression in the field  $F$  and its derivatives by a low-frequency filter will bring about a decrease in the dispersion. However, effects resulting from an equivalent deepening of the sources should be taken into account.

The Euler deconvolution can be applied not only to the gravity field strength  $g$  or to the magnetic field strength (or induction) elements  $X$ ,  $Y$ ,  $Z$ , but also to the calculable potentials. The DST (12) of the anomalous gravity potential  $V$  is

$$S^{(-N)}[V]_{O'} = -NV - (x - a)V_x - (y - b)V_y - (z - c)V_z \quad (41)$$

and for the magnetic potential  $W$ , it is

$$S^{(-N)}[W]_{O'} = -NW + (x - a)X + (y - b)Y + (z - c)Z, \quad (42)$$

where  $V_x$ ,  $V_y$  and  $X$ ,  $Y$  are horizontal components of the gravity and magnetic field strengths, whereas  $V_z = g$  and  $Z$  are vertical components. Usually one of these components is measured and by its distribution on a sufficiently large set of observation points we can calculate the values of the other components and the potential variations. The calculation of potentials  $V$  or  $W$  from gravity or magnetic field strengths is performed by means of a low-frequency filter suppressing the noise. When calculating a field strength component from other measured components the noise does not increase, while in the calculations of derivatives it rises significantly. Thus, by Euler deconvolution of  $V$  or  $W$  instead of field strengths, the noise effects can be avoided. The structural index  $N$  of  $V$  or  $W$  caused by a one-point source (Table 1) is lower by unity than that for the corresponding field strengths. The studies of Reid *et al.* (1990) on model and real data show that the dispersion of depth estimates increases with decreasing  $N$ . This fact lowers the useful effect of a deconvolution of  $V$  or  $W$ . The above-mentioned contradictory effects determine the priority of either the field strengths or the potential as a basic field for deconvolution in the different field cases.

The suggested technique of Euler deconvolution using DSTs enables a complete solution of the problem by solving the system of linear equations (31). It is also possible to obtain a solution for a prescribed value of the structural index  $N$ . For this purpose, we should exclude the fourth row in (31) and the terms of the fourth column should be



transferred to the right-hand side of the respective row. In this way the deconvolution is oriented towards detecting a definite type of source.

### *Two-point source anomalies*

Two-point sources are model sources whose dimensional geometrical parameters are completely represented by the coordinates of two singular points  $M_1(x_{01}, y_{01}, z_{01})$  and  $M_2(x_{02}, y_{02}, z_{02})$ . Many of the widely used interpretation models are two-point sources: a thick semi-infinite dike; a thin finite dike; a finite sill or effusive sleeve; a low-amplitude horst or graben structure; a finite contact or step in depth; a finite thin rod and pipe, etc. (Table 2). Two-point sources can be represented as a combination of two connected one-point sources of the same type with constant physical parameters equal in quantity and opposite in sign. For instance, a finite thin rod having a linear density  $m_1$  between points  $M_1$  and  $M_2$  is equivalent to two semi-infinite unidirectional and coaxial rods, the first having an initial point  $M_1$  and density  $m_1$ , the second having an initial point  $M_2$  and density  $-(m_1)$ . The corresponding analytical expression of the finite rod anomaly is a sum of the analytical expressions of the two anomalies caused by the two one-point sources (see examples in Appendix A).

Two closely located individual one-point sources, whose fields interfere, also form a two-point source. This type includes the models of a faulted thin bed, a low amplitude fault of a thick bed, two adjacent thin dikes, two successive thin steps, two opposite infinite contacts, etc. They form a two-point source which is not connected in one perturbing body.

All the above-mentioned two-point sources consist of two one-point sources of equal dimension  $d$ . They are homogeneous two-point sources, in contrast to the possible heterogeneous ones. The first type is considered here.

A two-point source can be characterized by its geometrical dimension  $d$  and relative size  $L = R_{M_1M_2}/z_{\min}$ , where  $R$  is the distance between the two singular points,  $z_{\min}$  is the depth of the shallower point. When  $L < 0.5$  approximately, then the respective source causes a field strength anomaly close to the anomaly of a one-point source. If  $L > 6$  approximately, then the two singular points are set wide apart and their anomalous effects can be interpreted separately.

An anomaly  $A$ , caused by a two-point source, is a sum of the anomalies  $A_1$  and  $A_2$  of its elementary one-point sources at points  $M_1$  and  $M_2$  with a dimension  $d$  and a corresponding structural index  $N$  (see (17)). The observed anomalous field  $F$  in the presence of a linear background trend  $\Phi$  (see (19)) is  $F = A_1 + A_2 + \Phi$ . The DST of  $F$  according to (12) and (13) is

$$S^{(-N)}[F]_{O'} = S^{(-N)}[A_1]_{O'} + S^{(-N)}[A_2]_{O'} + S^{(-N)}[\Phi]_{O'}. \quad (43)$$

If a CPS  $O'_1$  coincides with  $M_1$ , then  $S^{(-N)}[A_1]_{M_1} = 0$  according to (28). Therefore (43) takes the form

$$S^{(-N)}[F]_{M_1} = S^{(-N)}[A_2]_{M_1} + S^{(-N)}[\Phi]_{M_1}, \quad (44)$$

**Table 2.** Structural indices  $N$  of gravity and magnetic anomalies of two-point sources.

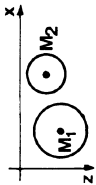
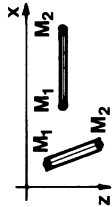
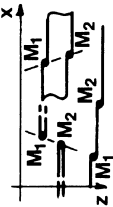
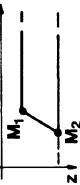
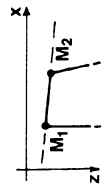
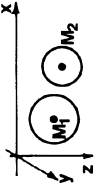
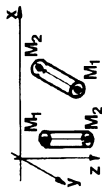
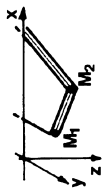
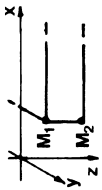
Name	Two-point source			Anomaly			
	Figure	Dimension $d$	Type $s$	Dimension $D$	Gravity Magnetic field	Potential $k = 0$	Strengths $k = 1$
Two lines of masses or dipoles, cylinders		1	1	2	G	0	1
Finite thin sill, dike, step, graben, horst, plate		2	1	2	G	-1	0
Faulted bed, two thin semi-infinite steps, dikes		2	1	2	G	-1	0
Finite step, contact		2	2	2	M	0	1
Thick dike, two semi-infinite contacts		3	1	2	G	-2	-1
Two point masses or dipoles, spheres		3	2	2	M	-1	0
		0	1	3	G	1	2
		0	2	3	M	2	3

Table 2. Continued.

Two-point source			Anomaly				
Name	Figure	Dimension $d$	Type $s$	Dimension $D$	Structural index $N$		
					Gravity Magnetic field	Potential $k = 0$	Strengths $k = 1$
Finite thin pipe, rod, two semi-infinite pipes, ..		1	1	3	G	0	1
Semi-infinite thin plate with two vertices		2	1	3	G	-1	0
Semi-infinite parallelepiped with finite thickness		3	1	3	G	-2	-1
		3	2	3	M	-1	0

which is an equivalent anomalous field of the one-point source at  $M_2$  with a structural index  $N' = N + 1$  (see (A3)) in the presence of a linear background trend  $\Phi' = S^{(-N)}[\Phi]_{M_1}$  (see (25)). The equivalent field (44) can be deconvolved by the procedures described above in the case of a one-point source. For this purpose, another CPS  $O'_2$  has to be selected, so that  $O'_2 = M_2$  and DST  $S^{(-N')}[S^{(-N)}[A_2]_{M_1}]_{M_2} = 0$  according to (28). In this way the DST of (44) can be written as

$$S^{(-N')}[S^{(-N)}[F]_{M_1}]_{M_2} = S^{(-N')}[S^{(-N)}[\Phi]_{M_1}]_{M_2}, \quad (45)$$

which is a linear function of the coordinates of the observation points  $P(x, y, z)$ . Thus,  $O'_1 = M_2$  and  $O'_2 = M_2$  bring about a linear function DST of second order,

$$C[F] = S[S[F]],$$

where according to (12) and (13)

$$\begin{aligned} C^{(-N)}[F]_{O'_1, O'_2} &= S^{(-N')}[S^{(-N)}[F]_{O'_1}]_{O'_2} \\ &= -N'S^{(-N)}[F]_{O'_1} - \mathbf{R}_{O'_2 P} \nabla_P (S^{(-N)}[F]_{O'_1}), \end{aligned} \quad (46)$$

with  $S^{(-N)}[F]_{O'_1} = -NF - \mathbf{R}_{O'_1 P} \nabla_P F$ ,  $N' = N + 1$ . It can be shown, after rearranging  $O'_1(a_1, b_1, c_1)$  and  $O'_2(a_2, b_2, c_2)$  in (46), that

$$C^{(-N)}[F]_{O'_1, O'_2} = C^{(-N)}[F]_{O'_2, O'_1}. \quad (47)$$

The first and second order derivatives of  $F$  are involved in the expression for  $C[F]$ .

The linearity of  $C[F]$  can be estimated by the residual dispersion  $Q^2[C]$  after linear regression defined by (29) for  $C$ . The condition for linearity of  $C[F]$  leads to the problem of minimizing the object function, i.e.

$$Q^2(a_1, b_1, c_1, a_2, b_2, c_2, N) = \min. \quad (48)$$

In contrast to (30), the problem of determining the seven unknowns in (48) is non-linear. It can be solved using linear operations by testing the minimum  $Q_m^2$  of (48) on a preset grid CPS  $O'(a, b, c)$  in the region of the expected source. If a CPS  $O'_1$  is given, then  $C[F]$  is a linear function of the coordinates of the other CPS  $O'_2$  (see (46)). For an accurately assigned structural index  $N$ , the subproblem,  $Q^2(a_2, b_2, c_2) = \min$ , can be solved within a square window by the system of normal equations

$$\Sigma t_{ij} p_j = r_i, \quad i = 1, 2, 3, \quad j = 1, 2, 3, \quad (49)$$

where  $p_1 = a_2$ ,  $p_2 = b_2$ ,  $p_3 = c_2$ ,  $t_{ij} = \Sigma \{E_m[S[D_i]]E_m[S[D_j]]\}$ ,  $m = 1, 2, \dots, K$ ,

$$r_i = \Sigma \{E_m[G]E_m[S[D_i]]\}, \quad G = N'S[F] + xS[D_1] + yS[D_2] + zS[D_3],$$

$$S[D_i] = -N'D_i - (x - a_1)D_{i1} - (y - b_1)D_{i2} - (z - c_1)D_{i3}, \quad N' = N + 1,$$

$$D_i = \partial F / \partial v_i, \quad D_{ij} = \partial D_i / \partial v_j, \quad v_1 = x, \quad v_2 = y, \quad v_3 = z,$$

$$S[F] = S^{(-N)}[F]_{O'} \text{ (see (24))}, \quad E[H] \text{ is defined in (31).}$$

After solving system (49) the minimum  $Q_m^2$  has to be calculated using (35) in which  $C[F]$  is substituted for  $S[F]$ . In this way, on the CPS grid in the source region we obtain the distribution of  $Q_m^2(a, b, c)$ . The two equal minima of  $Q_m^2$  appear at the singular points  $M_1$  and  $M_2$ . The calculated  $C^{(-N)}[F]_{M_1, M_2}$  determines the coefficients of the background  $\Phi$ :

$$b_v = q_v / ((N + 1)(N + 2)), \quad v = x, y \text{ or } z, \quad (50)$$

$$B_0(x_c, y_c, z_c) = \{C_0 / (N + 1) + 2\mathbf{bR}_{O_c M_c}\} / N,$$

where  $M_c$  is the midpoint between  $M_1$  and  $M_2$ ,  $O_c(x_c, y_c, z_c)$  is the central point of the window,  $C_0$  and  $q_v$  are regression coefficients calculated as in (34). The solution quality can be estimated after reproducing system (49) at one of the two minimum points obtained and determining the dispersion of the results for the coordinates of the other point according to (36) for  $U = 3$ . In the case of 2D deconvolution in the  $XOZ$ -plane, the respective  $2 \times 2$  system derives from (48), excluding the second row and column.

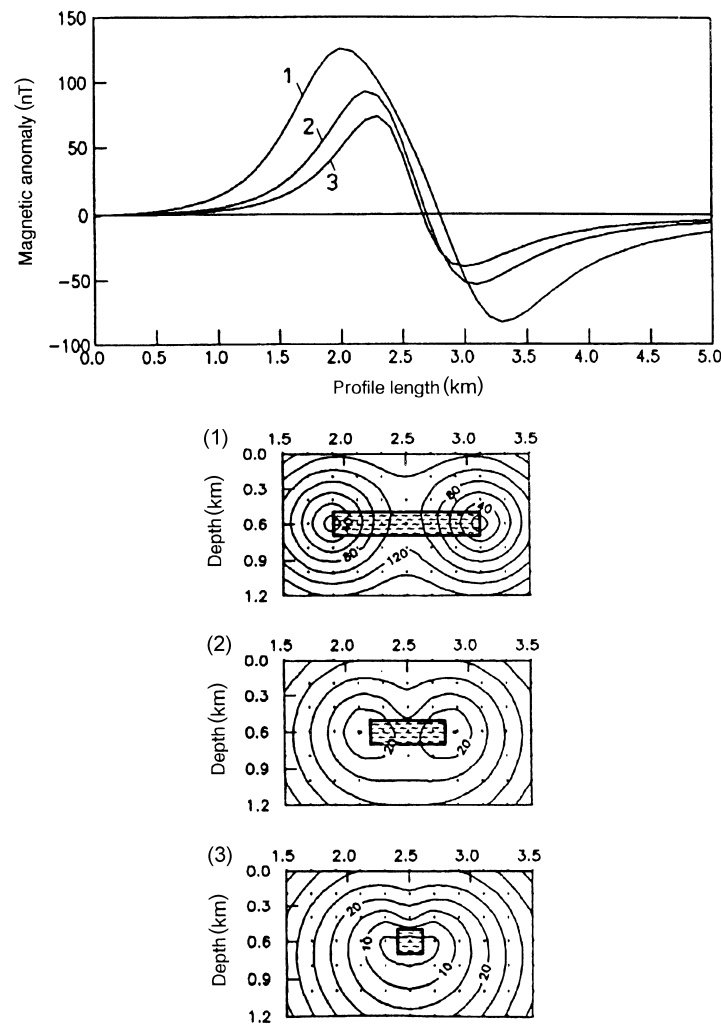
Results from this linear technique applied to model and real magnetic data are shown in Figs 3–6, 8b and 9b. By the fairly wide-meshed CPS grid the position of the two minima can be specified graphically. This approach is appropriate for 2D problems solved in one wide window covering the observed anomaly. In 3D problems, the necessary CPS grid increases many times thus lengthening the calculation time and complicating the graphic estimate of the results.

A full, direct and rapid solution to (48) is obtained by applying an optimization method in non-linear problems. The well-known method of Levenberg–Marquardt (Gill, Murray and Wright 1981) is suitable. Functions  $C[F]$  (see (46)) and their linear regression have a simple algebraic form so that the minimization of  $Q^2$  (see (48)) in a square or linear window takes little calculation time. The problem can be solved for the complete set of unknowns or only for the coordinates of the two singular points using a given structural index  $N$ . The assessment of the solution quality can be made as shown by Leite and Leao (1985). In contrast to the model optimization, the Euler deconvolution does not require the assignment of geometrical and physical parameters to the source. Results obtained by this approach in 2D interpretation problems are shown in Figs 7–9.

The proposed techniques of Euler inversion can be applied either to the measured components of the gravity and magnetic fields or to the calculated potentials. In the first case the derivatives up to the second order must be available. In the case of potentials as a basic field for inversion, derivatives up to the first order must be used. The decrease in the derivative order helps to avoid negative effects due to random noise (Fig. 6).

### Implementation

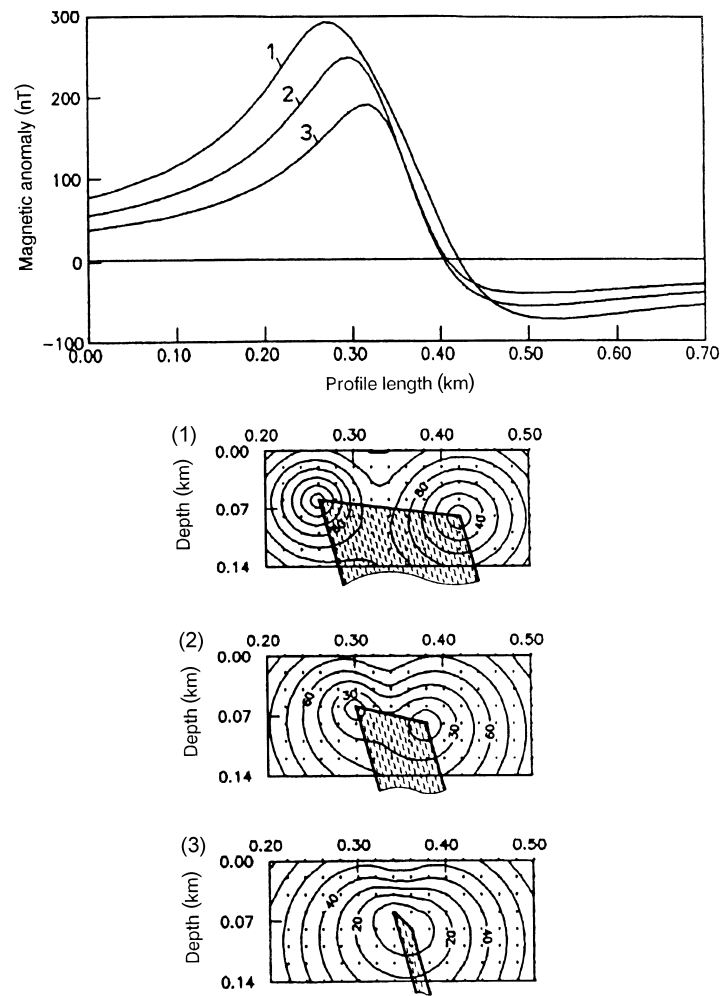
The DST technique of Euler deconvolution oriented to one-point source approximations employs data prepared as suggested by Thompson (1982) in two dimensions and



**Figure 3.** Vertical maps of the residual standard  $Q_m(O')$  after Euler deconvolutions of  $S_2[\Delta T]$  transformations of 2D magnetic anomalies  $\Delta T$  caused by thin sills ( $d = 2$ ) with different width/depth ratios: (1) 3.6, (2) 1.0, (3) 0.3.

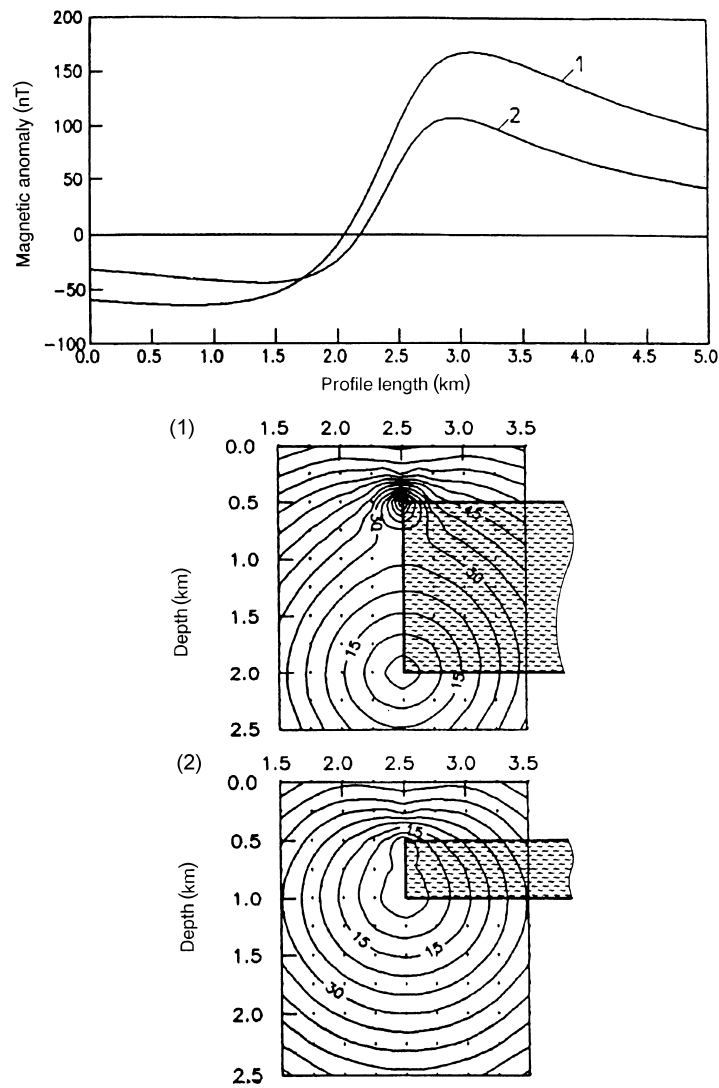
by Reid *et al.* (1990) in three dimensions. The window size must be chosen to be greater than the depth of the sources under estimation. The window should include a sufficient number of points, in all cases more than 7 and the greater, the better. The window size can be determined experimentally on the basis of the solution quality. In the case of quadratic windows a preliminary test for non-two-dimensionality of the deconvolved field according to (40) is useful.

The coordinates of the singular point  $M$ , the structural index  $N$  and the coefficients of a possible linear trend result from the solution of the  $4 \times 4$  system (31) in the 3D case



**Figure 4.** Vertical maps of the residual standard  $Q_m(O')$  after Euler deconvolutions of  $S_3[\Delta T]$  transformations of 2D magnetic anomalies  $\Delta T$  caused by thick dikes ( $d = 3$ ) with different width/depth ratios: (1) 2.3, (2) 1.2, (3) 0.3.

or from the reduced  $3 \times 3$  system in the 2D case. These are optimum results characterized by their standard deviations  $\sigma$  (see (36)). The coordinate estimates are acceptable if their relative standard deviations (in relation to the estimated depth) do not exceed a level chosen empirically. Reid *et al.* (1990) recommend acceptance levels between 15% and 25%, which increase with decreasing structural index  $N$ . The DST technique yields, in addition, an optimum result for  $N$ , whose reliability has to be estimated on the basis of its standard deviation and value. An admissible standard deviation of  $N$  is less than approximately  $|\pm 0.25|$ . The value obtained for  $N$  is acceptable if it corresponds to a real geometrical dimension  $d$  (between 0 and 3) of the



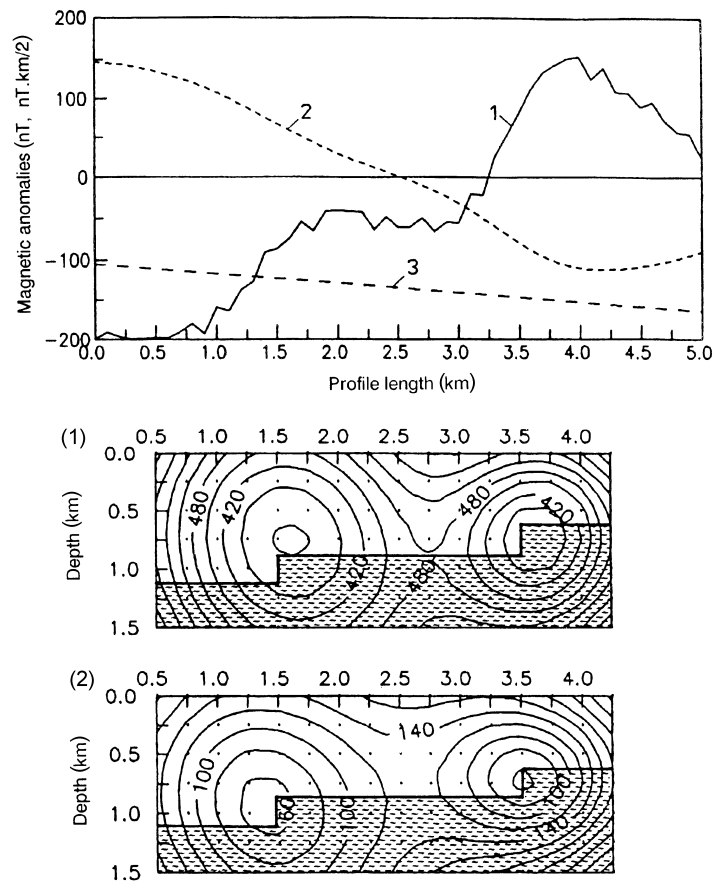
**Figure 5.** Vertical maps of the residual standard  $Q_m(O')$  after Euler deconvolutions of  $S_3[\Delta T]$  transformations of 2D magnetic anomalies  $\Delta T$ , caused by finite contacts ( $d = 3$ ) with different thickness/depth ratios: (1) 3.0, (2) 1.0.

sources. Thus, taking into account (7) and (17), a second acceptance criterion,

$$(s + k - 3) - \delta < N < (s + k - 3) + D + \delta, \quad (51)$$

has to be satisfied, where  $s$ ,  $k$  and  $D$  are defined in (3) and (7) and given in Tables 1 and 2,  $\delta < 0.5$  is a positive parameter, which must be chosen according to the desired extent of the rigid condition (7) for the calculated  $N$ . If the estimated  $N$  is outside these limits,

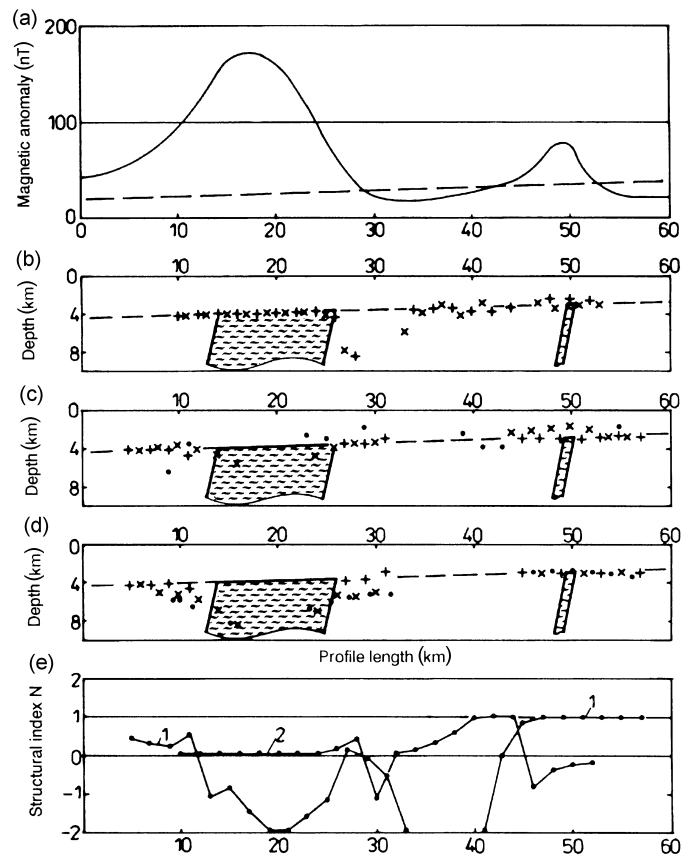




**Figure 6.** Vertical maps of the residual standard  $Q_m(O')$  after Euler deconvolutions of  $S_2[\Delta T]$  transformations of a magnetic anomaly  $\Delta T$  (1) and  $S_2[W]$  of the calculated potential  $W$  (2). The anomalous field caused by two thin steps ( $d = 2$ ) consists of a linear background trend (3) and random noise.

then all results obtained in the given window are unreal. The best quality results correspond to an optimum  $N$  close to the integers in the above interval. The estimated  $d = s + k - N$  (see (17)) determines the geometrical type of the source (Table 1). After a successful deconvolution the coefficients of a possible linear background trend can be calculated from (33) and (34). Successive deconvolutions in overlapping windows make it possible to select a final result within the range of an anomaly.

The DST technique of Euler deconvolution oriented to two-point source approximations can be implemented along with the above one-point source procedures. For this purpose the second derivatives of the basic deconvolved field  $F$  also have to be calculated. On the basis of the measured or calculated first derivatives  $D_1 = \partial F / \partial x$ ,  $D_2 = \partial F / \partial y$  and  $D_3 = \partial F / \partial z$  (see (31)), all second derivatives in (46)–(49) can be



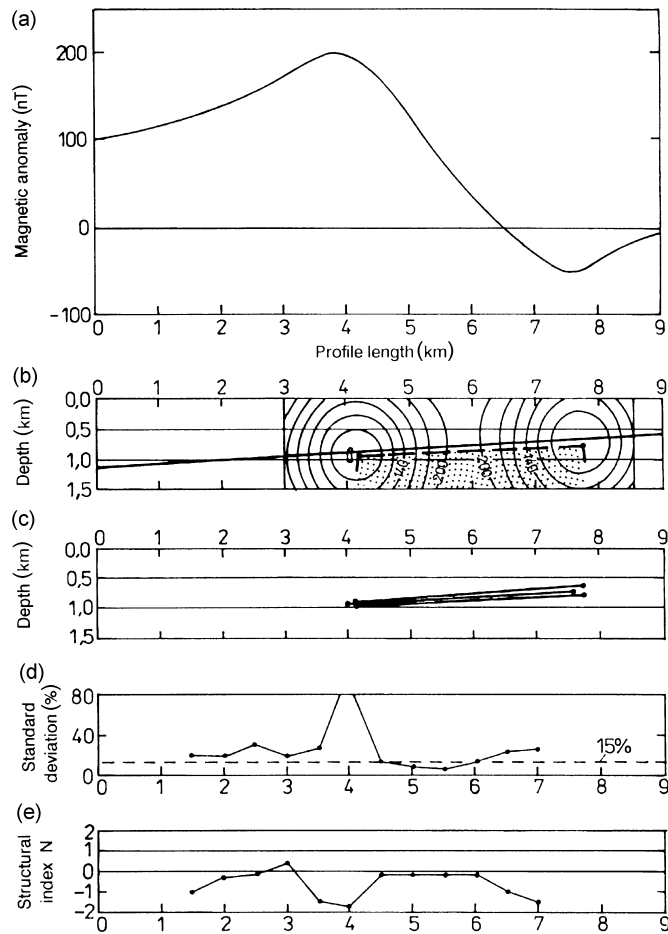
**Figure 7.** Model estimates of the depth of a thick dike and a thin dike, using three techniques of Euler deconvolution in overlapping windows: (+) DST with calculated structural indices  $N$ ; (x) DST with a prescribed  $N$ ; (•) direct deconvolution with a prescribed  $N$ . (a) 2D magnetic anomaly  $\Delta T$  (—) consisting of a linear background trend (---), data interval 0.5 km. (b) Mean depths estimated by the procedures for two-point sources, window length 18 km,  $N = 0$ . (c) and (d) Depths estimated by the procedures for one-point sources, window length 8 km,  $N = 0$  in (c) and  $N = 1$  in (d). (e) Curves of the calculated  $N$ : 1 — in the cases (c) and (d), 2 — in the case (b). The depth and  $N$  estimates are shown under the central point of the respective window.

calculated simply as horizontal derivatives of  $D_1, D_2, D_3$ . For a harmonic field  $F$

$$D_{11} = \partial D_1 / \partial x, \quad D_{12} = D_{21} = \partial D_2 / \partial x, \quad D_{13} = D_{31} = \partial D_3 / \partial x,$$

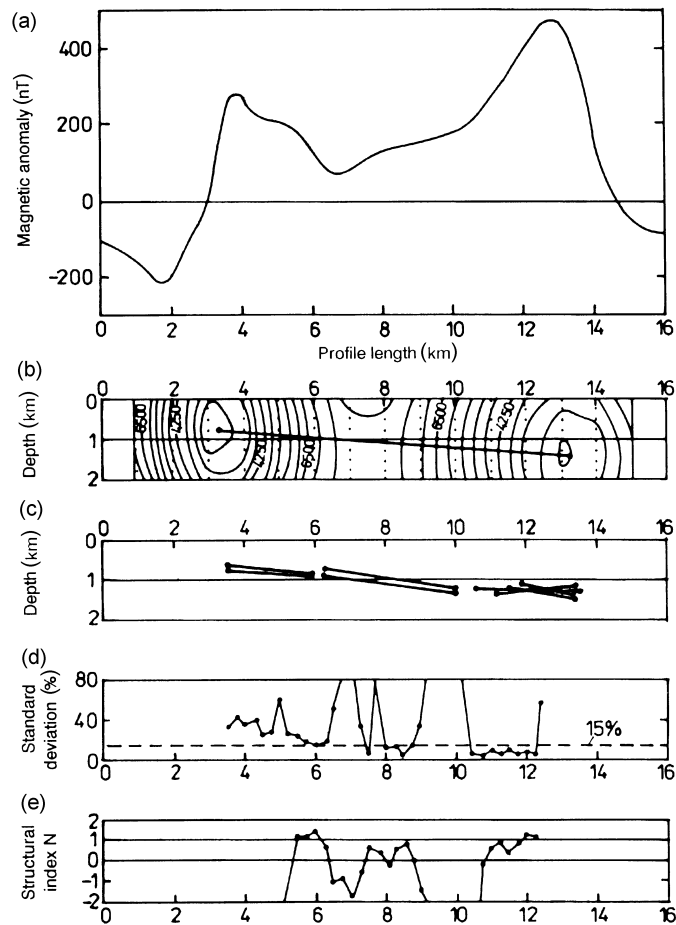
$$D_{22} = \partial D_2 / \partial y, \quad D_{23} = D_{32} = \partial D_3 / \partial y, \quad D_{33} = -(D_{11} + D_{22}).$$

In the case of considerable random noise, an appropriate filter has to be applied. Another approach is to calculate the potentials  $V$  or  $W$  using integral or spectral techniques.



**Figure 8.** (a) Aeromagnetic profile 'Surnevo' interpreted using DST. (b) Vertical map of the residual standard  $Q_m(O')$  after Euler deconvolutions of  $S_3[\Delta T]$  profiles with a prescribed structural index  $N = 0$  ( $d = 3$ ), window interval (2—9) km. The continuous line marks the basement surface, the dashed line is the result for the upper surface of the perturber. (c) Results obtained using DST with calculated  $N$ , window length 6 km. (d) Curve of the relative standard deviations of the depth estimates obtained in overlapping windows. (e) Curve of the calculated  $N$  addressed to the central point of the respective window.

After preparing the grid of necessary data, the window size must be chosen. The minimum size is equal to the depth plus the width or thickness of the expected two-point sources. The coordinates of the two singular points, the structural index  $N$  and the background coefficients result from the solution of (48) or (49). The reliability of the estimates obtained is tested using the two above-described acceptance criteria jointly. The first criterion of the relative standard deviations in the coordinate estimates is formed empirically. The second criterion of the real  $N$  estimate (51) is defined more



**Figure 9.** (a) Aeromagnetic profile 'Meden bouk' interpreted using DST. (b) Vertical map of the residual standard  $Q_m(O')$  after Euler deconvolutions of  $S_2[\Delta T]$  profiles with a prescribed index  $N = 1$  ( $d = 2$ ), window interval (1—15) km. As a result the average plane of a thin inclined plate between the two minima of  $Q_m$  is outlined. (c) Depth, width and slope estimates of the plate elements, window length 6 km. (d) Curve of the relative standard deviations of the depth estimates obtained in overlapping windows. (e) Curve of the calculated  $N$  addressed to the central point of the respective window.

strictly. After a successful deconvolution in a given window, the type of perturber can be evaluated by the interpreter, taking into account the estimated dimension  $d = s + k - N$  (see (17); Table 2), the depths of the two singular points and the distance between them, as well as the configuration of the deconvolved anomaly. The deconvolution can also be carried out with a prescribed structural index  $N$  (Table 2).

A parallel Euler deconvolution using DST techniques oriented to one-point and two-point source approximations makes it possible to select the best reliable results in

different field cases. If gridded data are available in an area of prolonged anomalies, then 2D deconvolution along a series of cross-profiles yields more stable results. This approach was used in the model and field examples shown in Figs 3–9.

## Model examples

### *Curves of differential similarity transformations*

Figure 2 illustrates curves of model 2D gravity and magnetic anomalies and their DSTs calculated according to (12) in relation to several CPS  $O'$  and prescribed indices  $u$  or respective degrees  $n$  of Euler homogeneity (see (5)).

Figure 2a presents a gravity model of a perturbing body with an approximately isometric cross-section. The curves  $S_1[\Delta g]$ , according to their dipole equivalent sources (see Appendix A), have the form of magnetic anomalies. The amplitude and sign of the main extrema depend on the position of the CPS in relation to the causative body. In the case of CPS 2, the  $S_1[\Delta g]_{O'_2}$  curve has a minimum amplitude. This is an indication that point  $O'_2$  is close to the central point of the body.

The curves of  $S_3[\Delta g]$  transformations are shown in Fig 2b. They have extrema over the side planes of the causative body. When the CPS are inside the convex homogeneous body (point 1) or in immediate proximity (point 2), the respective curves 1 and 2 have only positive values. If point  $O'$  is farther away from the body (point 3), then a part of the curve has negative values. These results are in accordance with the physical interpretation of  $S_3[\Delta g]$  transformations (see (A6)). Thereby we can define a sufficient indication for determining the CPS (in this case point 3) as being outside the causative body.

Figure 2c shows a magnetic model with a thin sill as a causative body. The sill approximates to a two-point source of dimension  $d = 2$  and surface dipole density of index  $u = 2$ . Several transformations  $S_2[\Delta Z]$  towards the CPS around the right edge of the sill are plotted. As can be seen, the curves have their extrema over the left edge point. In the right part of the profile the curves have weaker variations depending on the location of the CPS in relation to the right edge point. Curve 2, which corresponds to CPS 2 coinciding with the edge point, is the smoothest. In this case the effect of the right singular point of the thin sill is suppressed at the maximum and curve 2 approximates to the field  $\Delta Z'$  due to a line of dipoles through the left edge point. The properties pointed out serve as a basis for recognizing when the CPS coincides with the edge points of the sill.

Figure 2d illustrates DST of a magnetic anomaly  $\Delta T$  along a line over a thick dike model. In this case, transformations  $S_3[\Delta T]$  are of interest, due to the dimension  $d = 3$  of the causative body. Only three of the many possible curves towards different CPS are plotted. Obviously curve 2, obtained when CPS 2 coincides with the left edge point of the dike, has the least variations. This is due to the complete suppression of the effect of this singular point in the calculated field  $S_3[\Delta T]$  (see Appendix A). What remains is the effect of the other singular edge point of the two-point source. In this case, curve 2

has the form of an anomaly  $\Delta T'$  caused by a thin dike along the right plane of the thick dike. Similarly, if the CPS coincides with the right edge point of the dike, then  $S_3[\Delta T]$  is a field of a thin dike along the left plane of the thick dike. Thus, an indication of the coincidence of a CPS with an edge point is that the respective  $S_3[\Delta T]$  transformation belongs to the family of anomalies caused by a thin dike, which is a one-point source. This can be evaluated by the quality of Euler deconvolution applied to the calculated  $S_3[\Delta T]$ .

#### *Distributions of residual standards $Q_m$*

Figures 3–6 show 2D magnetic profiles,  $\Delta T$ , of two-point sources having various relative sizes, and the respective distributions of the minimum residual standards,  $Q_m = +(Q_m^2)^{1/2}$ , obtained on a prescribed grid of CPS  $O'_1$  after solving (49). The value of  $Q_m(O'_1)$  is an estimate of the minimum possible deviation of DST  $C[\Delta T]_{O'_1, O'_2}$  (see (46)) from a linear function along the magnetic profile.

The model sources in Figs 3.1, 2 are sills dimension approximating  $d = 2$ . The respective transformations,  $C[\Delta T] = S_1[S_2[\Delta T]]$ , were calculated and their residual standards  $Q_m$  plotted. As can be seen, two equal minima of  $Q_m$  appear at the edge points. The sharpness of the minima decreases as the relative size of the sill decreases, until the third case (Fig. 3.3), where the model body is primarily a one-point source (a line of dipoles) and  $Q_m$  reaches a minimum at the same depth.

Results with the same characteristics were obtained for magnetic models of thick to thin dikes (Fig. 4). For the source dimension  $d = 3$ , the respective transformations  $C[\Delta T] = S_2[S_3[\Delta T]]$ , were calculated and their linearity estimated. The standards  $Q_m$  obtained have two minima located at the edge points of the dike (Figs 4.1, 2). For the thin dike model (Fig. 4.3) the distribution of  $Q_m$  has a lower gradient and the two minima converge into a wider minimum.

The experimental results on models of magnetic contacts ( $d = 3$ ) are shown in Fig. 5. The distribution of  $Q_m$  has two minima located at the edge points of the contact. The two minima are equal in value according to the theory (see (47)), but the lower one is less sharp. This means that the resolution capacity of the deconvolution for the deeper edge point decreases, as would be expected in every inversion of such an anomaly. With decreasing contact thickness (Fig. 5.2), the minima tend to converge to a point close to the midpoint of the contact.

A complicated model of an anomalous field containing a regular side effect and random noise is shown in Fig. 6. Two thin steps on a magnetic surface create a low-intensity anomaly  $\Delta T$ . A linear trend having a gradient of 10 nT/km and 5% relative standard noise are added to the anomaly. The two-point source has a relative size  $L = 2.7$  and a dimension approximating  $d = 2$ . The respective transformations,  $S_2[\Delta T]$ , towards the CPS grid shown are subjected to Euler deconvolution using DST. The  $Q_m$ -map of  $C[\Delta T] = S_1[S_2[\Delta T]]$  obtained forms two minima close to the steps (Fig. 6.1). The observed displacement is due to the noise in the model data. In order to improve the result, the calculated potential  $W$  was given as a basic field for

deconvolution. In this case the DST,  $C[W] = S_1[S_2[W]]$ , involves only first derivatives of  $\Delta T$  thus avoiding the use of more strongly noise-affected second derivatives of  $\Delta T$  in  $C[\Delta T]$ . This useful effect can be seen in the closer location of the minima to the midpoints of the two thin steps.

#### *Depth estimates in overlapping windows*

The quality of the depth estimates obtained by a 2D Euler deconvolution using DST and a direct approach (Thompson 1982) was tested on a magnetic profile  $\Delta T(s=2, k=1)$  of two anomalies caused by two adjacent thick and thin dikes in the presence of a linear background trend (Fig. 7). The first source is two-point, having a dimension  $d=3$  and a corresponding structural index  $N=0$  of its anomaly (Table 2), the second source approximates a one-point source having dimension  $d=2$  and corresponding structural index  $N=1$  (Table 1). The dikes outcrop on an inclined surface of the 'basement' at an average depth of 3.8 km for the thick dike and 3 km for the thin dike. The model data  $\Delta T$  were calculated at intervals of 0.5 km along the profile (Fig. 7a).

Two windows, different in size, were used. The first window, 8 km long (twice the depth), corresponds to the one-point source approximation, and the second window, 18 km long (twice the depth plus the width of the thick dike), corresponds to the two-point source. The DST techniques were performed with calculations of the optimum structural index  $N$  and separately with a prescribed  $N$ . The depth estimates obtained (Figs 7b,c,d) are shown under the central point of the respective window. For the two-point source estimates, the mean depth of the two singular points is plotted. All depth estimates shown are selected according to an acceptance level for a 15% relative standard deviation. The calculated structural indices  $N$  have standard deviations within  $\pm 0.2$ . Their acceptance interval is chosen between  $-0.5$  and  $2.5$  according to the criterion (51).

Results obtained by DST techniques oriented to detection of two-point sources (48) are shown in Figs 7b,e. In the windows over the thick dike the depth estimates are correct and the calculated indices  $N$  maintain the correct value of zero. The corresponding results over the thin dike are less stable because of the smooth object function (see Fig. 4). The depth estimates of the two closely spaced singular points of the thin dike may differ significantly but their mean depth approximates the real depth of the dike. In the intermediate interval of the profile, where two anomalies interfere, the results obtained are close to the mean depth of the two dikes. The indices  $N$  increase from zero to unity thus reflecting the transition from the thick dike source to two thin dikes (magnetic effects away from the thick dike approximate the effects of a thin dike). When the windows are located over the thin dike, the structural index again approximates zero which is indicative of an infinite dike with a small finite width.

The deconvolutions performed under the assumption of one-point sources yield depth estimates shown in Figs 7c,d. The DST technique with calculated  $N$  (see (31)) gives reliable depth estimates for the thin dike and for the two edge points of the thick

dike. In the thick dike case, these results were obtained from windows located round the periphery of the dike, where the calculated  $N$  are close to zero. Over the thick dike, all indices  $N$  have high negative unreal values and the respective depth estimates were not accepted according to the second criterion (51).

The direct and DST techniques employing a prescribed index  $N$  were tested with  $N = 0$  (Fig. 7c) and  $N = 1$  (Fig. 7d). The first index corresponds to anomalies of one-point sources with dimension  $d = 3$ , such as contacts along the side planes of the thick dike with singular points at the edge points of the dike. The second index corresponds to the thin dike ( $d = 2$ ) anomalies. As can be seen and would be expected, the depth estimates over the respective type of source are accurate, on the average, whereas over the other source considerable unidirectional deviations take place. The influence of the linear background trend on the results from the direct Euler deconvolution is expressed in the comparatively higher dissipation in the depth estimates, particularly for  $N = 0$ . All results given satisfy the acceptance criterion of a relative standard deviation less than 15%, but nevertheless some depth estimates deviate from the real depth more than is acceptable (Figs 7c,d). Therefore, the criterion of the relative standard deviation is necessary but not sufficient for the selection of reliable depth estimates. This disadvantage is overcome in the DST techniques by the possibility of applying a second acceptance criterion (51), formulated on the basis of the estimated structural indices (Figs 7b,c,e).

## Field examples

### *Magnetic anomaly: 'Surnevo'*

An aeromagnetic profile  $\Delta T$  across an anomaly near the town of Stara Zagora in South Bulgaria is shown in Fig. 8. The profile, having a  $20^\circ$  azimuth, lies in the central part of the Sredna Gora structural zone where the main sources of magnetic anomalies are gabbro-monzonite-granite intrusions and basalt-andesite and trachybasalt-latitude effusions. The profile, containing 37 observation points at intervals of 0.25 km, was interpreted by DST techniques oriented to two-point source approximations.

After experimental tests, the best results were obtained from overlapping windows 6 km in length (25 observation points). The calculated indices  $N$  (Fig. 8e) have standard deviations within  $\pm 0.2$  and real values approximating zero. This means that the dimension  $d$  of the causative body approximates  $d = 3$ , according to (17). Such a dimension in 2D problems corresponds to a dipping dike or to a finite contact in depth (Table 2). The coordinate estimates of the two edge points were selected using an acceptance level for a 15% relative standard deviation (Fig. 8d) and applying the criterion (51) of  $N$  calculated in the interval  $-0.5 < N < 2.5$ . The reliable results obtained in this way are shown in Fig. 8c, where the two edge points are connected by a straight line. According to these results a thick body with vertical extension is more probable as a causative body than a contact. The upper surface of this body is 3.5 km wide and lies at an average depth of 0.7 km in the north up to 0.9 km in the south. The



same estimates were obtained by the DST technique of linear procedures (49), employing data in one larger window between observation points 2.0 km–9.0 km (Fig. 8a). For the prescribed correct value of  $N = 0$ , the calculated distribution of the residual standards  $Q_m$  has two minima pointing to the edge points of the causative body (Fig. 8b).

The results obtained for the depth and dip of the upper surface of the magnetic perturber are in accordance with the interpolated geological data (Tectonic Map of Bulgaria, Technika, Sofia, 1971) for the surface of the Upper Eocene basement shown by a thick line on Fig. 8b. The most probable interpretation is that an intrusive body outcrops on the basement surface in this superimposed depression.

#### *Magnetic anomaly: 'Meden bouk'*

Near the town of Kroumovgrad in the Eastern Rhodopes, Southeast Bulgaria, a wide magnetic anomaly surrounded by negative extrema is observed. An aeromagnetic profile  $\Delta T$ , containing 64 points at 0.25 km intervals along a line having an azimuth  $120^\circ$ , is shown in Fig. 9a. According to geological assumptions the causative body is a wide ultrabasic plate.

The magnetic profile was first deconvolved in one 15 km long window comprising almost the entire anomaly shown. A structural index of value  $N = 1$  was prescribed. It corresponds to a thin plate model with dimension  $d = 2$  (Table 2). The respective residual standards  $Q_m$  of DST  $C[\Delta T] = S_1[S_2\Delta T]$  (see (49)) were calculated on the CPS grid shown and plotted (Fig. 9b). As a result the average plane of an inclined plate between the two minima of  $Q_m$  is outlined. The depth increases from 1 km in the west up to 1.6 km in the east, the width of the plate being 10 km.

An analysis of the magnetic profile shows that the plate is probably discontinuous, displaced or has a variable thickness or magnetization in some intermediate intervals. Therefore the DST technique (48) was applied in overlapping windows each having a length of 6 km (25 points), according to the depth and expected width of the plate elements. The indices calculated in successive windows (Fig. 9e) have real values among which those between 0.5 and 1.25 are dominant. Therefore the magnetic body has a dimension approximating  $d = 2$ , according to (17). In this way the supposition of a magnetic perturber with a small thickness in relation to its width is confirmed.

The solutions shown in Fig. 9c have been selected according to the criterion for the relative standard of the coordinate estimates (15%) and criterion (51) for the real structural index between  $-0.5$  and  $2.5$  in the problem solved. As can be seen, the possible intermediate singular points of the source are located in the intervals around the 6th kilometre and between the 10th and 12th kilometres along the magnetic profile. The position of the two final points of the combined plate and the average dip remain the same as in Fig. 9b.

The coordinate estimates thus obtained can be used as supporting points in further construction and optimization of a more complicated magnetic model.

## Conclusions

The Euler homogeneity is an inherent property of gravity and magnetic anomalous fields. It is a basis for developing methods of gravity and magnetic inversion aimed at the detection of singular points of the anomalous fields. The differential similarity transformations are an appropriate means for the realization of Euler deconvolution.

Some limitations of Euler deconvolution can be overcome by the use of DST. A joint solution of the linear problem for the coordinates of one-point sources and the structural index of the deconvolved anomaly in the presence of a linear background trend is possible. Furthermore, the source approximations can be extended to more complicated two-point sources. The selection of reliable results is improved, involving a second acceptance criterion on the basis of the calculated structural index.

The proposed DST techniques for Euler inversions using either linear or non-linear systems of equations are easily implemented on a PC. The computational efficiency does not depend greatly on the type of these equations. For a non-linear inversion, the object function (48) has a simple algebraic form and its multiple calculation in the process of an automated optimization does not create technological problems.

The 2D model and field examples presented confirm the theoretical formulations of the DST techniques of Euler deconvolution and show their effectiveness in different cases of one-component magnetic data. The depth, horizontal coordinates and type of widely spread magnetic and gravity perturbations (Tables 1, 2) can be estimated independently of the width/depth ratio. Data on the density contrast or on the vector of magnetization are not necessary. The DST techniques proposed are also useful for joint rapid interpretation of data acquired from magnetic and gravity gradiometric measurements, as well as from three-component magnetic measurements.

## Acknowledgements

I thank the Committee of Geology and Mineral Resources at the Council of Ministers of the Republic of Bulgaria for providing the field data and permission to publish the results. I am also grateful to Dr A.Tzvetkov for fruitful discussions on the field examples.

I am especially indebted to the PACE Foundation for the support which made it possible to present this paper at the 56th annual meeting of the EAEG in Vienna. I thank the reviewers for their competent remarks on the scientific content.

## Appendix A

### Equivalent sources of differential similarity transformations

Transformations  $S[A]$  (see (12)) can be treated as calculable fields of the corresponding transformed original sources. The type, quantity and distribution of

these equivalent sources becomes apparent after appropriate processing and analysis of the analytical expressions of  $S_u[A(x, y, z)]_{O'}$  for different choices of their parameters, the index  $u$  or degree  $n$  and coordinates  $a, b, c$  of a central point of similarity (CPS)  $O'$ . For the analytical expressions of gravity and magnetic anomalies used below, see Telford *et al.* (1990).

#### Transformations of gravity anomalies

The potential  $V$  of the field created by a mass  $m$  at point  $M$  is given by  $V(P) = \gamma m/r_{MP}$ . The source of  $V(k=0)$  is a mass ( $s=1$ ) with quantity  $m(u=0)$  at the point figure  $M(d=0)$ . The degree of homogeneity  $n$  of  $V$  is  $n=0-1-0=-1$  (see (5)). After substitution of the above expression for  $V$  in (12) with a parameter  $u=d=0$ , we have

$$S_0[V(P)]_{O'} = -V(P) - \mathbf{R}_{O'P} \nabla_P V(P) = \gamma m \mathbf{R}_{O'M} \nabla_M (1/r_{MP}). \quad (\text{A1})$$

This is an expression of the potential caused by an equivalent 'gravity' dipole at point  $M$  with a moment

$$\boldsymbol{\mu} = m \mathbf{R}_{O'M}, \quad (\text{A2})$$

where  $\mathbf{R}_{O'M}$  is the distance vector between points  $O'$  and  $M$ . If a chosen CPS  $O'$  coincides with the source point  $M$ , then  $\mathbf{R}_{O'M} = 0$  and therefore  $S_0[V]_M = 0$  at all observation points  $P$ . The type of the equivalent source is  $s'=2$  (dipole) and the degree of homogeneity of  $S_0[V]$  is  $n'=0-2-0=-2$ , as it proceeds directly from (A1) and (A2). In comparison with the degree  $n=-1$  of  $V$ , the degree  $n'$  is less by unity. The structural index (SI) is respectively greater by unity, or

$$N' = N + 1, \quad (\text{A3})$$

where  $N=-n$  is the SI of the original anomaly, and  $N'=-n'$  is the SI of its transformation.

If a set of point masses  $m_j$  at points  $M_j$  creates a potential  $V = \Sigma V_j, j=1, 2, \dots, q$ , then the equivalent sources of  $S_0[V]$  are dipoles at points  $M_j$  with moments  $\boldsymbol{\mu}_j = m_j \mathbf{R}_{O'M}$ , according to (A2). In the case of continuously distributed volume masses in a solid figure  $B$  with density  $\rho = dm/d\tau$ , each elementary mass  $dm$  in an elementary volume  $d\tau$  becomes an elementary dipole with a moment  $d\boldsymbol{\mu} = dm \mathbf{R}_{O'M}$ , according to (A2). The density of these equivalent sources of  $S_0[V]$  is  $\mathbf{J} = d\boldsymbol{\mu}/d\tau$ , or

$$\mathbf{J}(M) = \rho(M) \mathbf{R}_{O'M}. \quad (\text{A4})$$

The corresponding integral of  $S_0[V]$  may be decomposed (Gauss) as

$$S_0[V] = \gamma \int_B \mathbf{J}(M) \nabla_M (1/r_{MP}) d\tau = \gamma \oint_C J_v(M) ds/r_{MP} - \gamma \int_B \nabla \cdot \mathbf{J}(M) d\tau/r_{MP}, \quad (\text{A5})$$

where  $C$  is the surface of  $B$ ,  $\mathbf{v}$  is the outward normal to the elements  $ds$  of  $C$ ,  $J_v(M) = \rho(M) (\mathbf{R}_{O'M})_v$ ,  $\nabla \cdot \mathbf{J}(M) = \mathbf{R}_{O'M} \nabla_M \rho(M) + 3\rho(M)$ . In the case of  $\rho(M) = \text{const}$ , the second integral results in  $3V(P)$ . Thus, taking into account (13) and (A5),

we have

$$S_0[V] + 3V = S_3[V] = \gamma \oint_C J_v(M) ds/r_{MP},$$

i.e. the equivalent sources of  $S_3[V]$  are masses on  $C$  with a surface density

$$J_v(M) = \rho(\mathbf{R}_{O'M})_v = \rho R_{O'M} \cos(\mathbf{R}_{O'M}, \mathbf{v}). \quad (\text{A6})$$

In 2D problems the elementary source is an infinite horizontal line of masses with a linear density  $\lambda(u = 1)$  and potential  $V(P) = 2\gamma\lambda \ln(1/r_{MP})$ , where point  $M$  is the line projection on the vertical normal plane. The transformation  $S_1[V]$  is equal to  $2\gamma\lambda \mathbf{R}_{O'M} \nabla_M (\ln(1/r_{MP}))$ , which is an expression of the potential created by a 'gravity' line of dipoles with a moment per unit length given by

$$\mu_0 = \lambda \mathbf{R}_{O'M}. \quad (\text{A7})$$

If  $O'(a, c)$  coincides with  $M(x_0, z_0)$ , then  $\mathbf{R}_{O'M} = 0$ ,  $\mu_0 = 0$  and  $S_1[V]_M = 0$  at all observation points  $P(x, z)$ . In the case of continuously distributed volume masses in a cylindrical solid body with a cross-section  $B_0$ , the equivalent sources of  $S_1[V]$  are lines of dipoles through  $B_0$  with a density  $\mathbf{J}_0(M)$ , defined by the right-hand side of (A4). If  $\rho = \text{const}$ , then  $S_3[V]$  has sources, distributed on the cylindrical surface with a density given by (A6).

All the above results for equivalent sources of  $S[V]$  are valid for  $S$  of each derivative of  $V$  of order  $k$  according to the equation  $S[\partial A/\partial v] = \partial S[A]/\partial v$  in (13).

The physical sense of  $S[A]$  can be shown more directly on some simple gravity models, such as rods, plates, steps, etc. For example, let  $A$  be a 2D anomaly  $g(x, 0)(k = 1, s = 1)$  caused by a finite step ( $d = 3$ ) with a density  $\rho(u = 3)$ , edge points  $M_1(0, z_1)$  and  $M_2(0, z_2)$  and thickness  $t = z_2 - z_1$ . For  $u = d = 3$ , the degree  $n$  of  $g$  is  $n = 3 - 1 - 1 = 1$  (see (6)). The respective  $S_3[g]$  transformation in relation to  $O' = M_1$  gives the expression

$$S_3[g]_{M_1} = g - x \partial g / \partial x + z_1 \partial g / \partial z = 2\gamma\sigma(\tan^{-1}(x/z_2) + \pi/2). \quad (\text{A8})$$

This is the expression of an anomaly  $g'(x, 0)$ , created by an equivalent thin step on the lower horizontal plane of the thick step with a surface density  $\sigma = \rho t$ . If  $O' = M_2$ , then  $S_3[g]_{M_2}$  takes the form  $2\gamma\sigma(\tan^{-1}(x/z_1) + \pi/2)$ , which is the gravity anomaly of a thin step on the upper plane. These results are in accordance with (A6), where, if  $O' = M_1$ , then  $(R_{M_1 M})_v$ , for all points  $M$  of the upper and side planes, is equal to zero, and for all points  $M$  of the lower plane, is equal to  $z_2 - z_1 = t$ , thus forming the equivalent density  $\rho t$ . If  $z_2 \gg z_1$  and  $|x| \ll z_2$ , then according to (A8),

$$S_3[g]_{M_1} \approx 2\gamma\sigma(x/z_2 + \pi/2). \quad (\text{A9})$$

Thus, in the case of a step with a large depth extent, if  $O' = M_1$ , then the respective transformation approximates a linear function of  $x$ . The degree of homogeneity  $n' = 0$  (see (A8)) is less than  $n$  by unity, because of the change of the dimension  $d = 3$  into  $d' = d - 1 = 2$  for the step planes as source figures of the equivalent surface masses ( $s' = s = 1$ ). This change of  $d$  is the other possible cause for relationship (A3).

### Transformations of magnetic anomalies

The elementary source of 3D magnetic anomalies is a dipole ( $s = 2$ ) at point  $M$  ( $d = 0$ ) with a magnetic moment  $\mu(u = 0)$ . Its potential  $W(P) = \mu \nabla_M(1/r_{MP})$  is a homogeneous function of degree  $n = 0 - 2 - 0 = -2$  (see (6)). For  $u = d = 0$ ,

$$S_0[W]_{O'} = -2W(P) - \mathbf{R}_{O'P} \nabla_P W(P) = \mathbf{R}_{O'M} \nabla_M (\mu \nabla_M (1/r_{MP})). \quad (\text{A10})$$

This expression gives the potential of a ‘magnetic’ quadrupole ( $s = 3$ ) at point  $M$  with a moment, depending on the distance vector  $\mathbf{R}_{O'M}$ . If  $O' = M$ , then  $\mathbf{R}_{O'M} = 0$  and  $S_0[W]_M = 0$  at all observation points  $P$ . The degree  $n' = -3$  of  $S_0[W]$  (A10) is less than  $n = -2$  of  $W$  by unity, due to the change in the type  $s' = s + 1$  of the equivalent source. Thus, (A3) is satisfied. In 2D problems, where a line of dipoles ( $d = 1$ ) is the elementary source with a moment per unit length  $\mu_0$  ( $u = 1$ ),  $S_1[W]$  has equivalent sources as a line of quadrupoles with a moment, depending on the vector  $\mathbf{R}_{O'M}$ , i.e. on the position of a chosen point  $O'$  with respect to the original line of dipoles.

The equivalent sources of  $S_u[A]$ , when  $A$  is a magnetic anomaly caused by continuously distributed dipoles in linear, surface or solid figures, can be determined on the basis of the above elementary results. Distributions of quadrupoles correspond to  $S_0[A]$  in 3D and to  $S_1[A]$  in 2D problems. When  $u = d$ , the equivalent sources of  $S_d[A]$  give simpler distributions. The following examples, concerning frequently used models for magnetic interpretation, are indicative.

(a) A finite thin pipe ( $d = 1$ ), between points  $M_1(0, 0, z_1)$  and  $M_2(0, 0, z_2)$  with a linear vertically oriented dipole density  $\lambda(u = 1)$  creates a magnetic anomaly,  $Z(x, 0, 0) = \lambda[z_1/(x^2 + z_1^2)^{3/2} - z_2/(x^2 + z_2^2)^{3/2}]$ , with degree  $n = 1 - 2 - 1 = -2$ . If  $O' = M_1$ , then

$$S_1[Z]_{M_1} = -2Z - x\partial Z/\partial x + z_1\partial Z/\partial z = \lambda(z_2 - z_1)(2z_2^2 - x^2)/(x^2 + z_2^2)^{5/2}, \quad (\text{A11})$$

giving the expression for a magnetic anomaly  $Z'(x, 0, 0)$ , caused by an equivalent dipole at point  $M_2$  with a moment  $\mu = \lambda(z_2 - z_1)$ . If  $O' = M_2$ , then the equivalent dipole is at  $M_1$ . In the case of a semi-infinite pipe ( $z_2 = \infty$ ),  $S_1[Z]_{M_1} = 0$ , according to (A11).

(b) A finite thin sill ( $d = 2$ ), between points  $M_1(0, z_0)$  and  $M_2(w, z_0)$  with a vertically oriented surface dipole density  $\sigma(u = 2)$ , creates an anomaly,  $Z(x, 0) = 2\sigma\{x/(x^2 + z_0^2) - (x - w)/((x - w)^2 + z_0^2)\}$ , of degree  $n = 2 - 2 - 1 = -1$ . If  $O' = M_1$ , then

$$S_1[Z]_{M_1} = -Z - x\partial Z/\partial x + z_0\partial Z/\partial z = 2\sigma w\{z_0^2 - (x - w)^2\}/\{z_0^2 + (x - w)^2\}^2. \quad (\text{A12})$$

This is an expression for an anomaly  $Z'(x, 0)$  due to a line of dipoles through the point  $M_2$  with a moment  $\mu = \sigma w$ . If  $O' = M_2$ , then the equivalent line of dipoles passes through point  $M_1$ . For a semi-infinite sill ( $w = \infty$ ),  $S_1[Z]_{M_1} = 0$  according to (A12).

(c) A finite contact ( $d = 3$ ), between edge points  $M_1(0, z_1)$  and  $M_2(0, z_2)$  with a vertically oriented dipole density (magnetization)  $\mathbf{J}(u = 3)$ , creates an anomaly,

$Z(x, 0) = 2J\{\tan^{-1}(x/z_1) - \tan^{-1}(x/z_2)\}$ , of degree  $n = 3 - 2 - 1 = 0$ . If  $O' = M_1$ , then

$$S_3[Z]_{M_1} = -x\partial Z/\partial x + z_1\partial Z/\partial z = 2J(z_2 - z_1)x/(x^2 + z_2^2), \quad (\text{A13})$$

which is an expression of a magnetic anomaly  $Z'(x, 0)$ , caused by a thin magnetic semi-infinite sheet on the lower horizontal contact plane with a vertically oriented surface dipole density  $\sigma = \mathbf{J}(z_2 - z_1)$ . If  $O' = M_2$ , then  $S_3[Z]_{M_2}$  is equal to the  $Z'(x, 0)$  anomaly of a magnetic sheet on the upper contact plane. When  $O'$  does not coincide with  $M_1$  and  $M_2$ , and does not lie on a contact plane, then  $S_3[Z]_{O'}$  is equivalent to a complicated anomaly  $Z'$  caused by three sheets along the three contact planes. For a contact with a large depth extent ( $z_2 \gg z_1$ ) and  $|x| \ll z_2$ , the DST  $S_3[Z]_{M_1} \approx 2Jx/z_2$ , i.e. this transformation approximates a linear function of  $x$  above the edge point  $M_1$ .

The results shown are also valid for anomalies  $Z$ ,  $H$  and low-intensity  $T$  of dipping and horizontal pipes, dipping or vertical thin dikes and sloping contacts with arbitrarily oriented magnetization. In the broader case of sources distributed in solid figures with a constant magnetization  $\mathbf{J}$  and a complicated shape, the respective integral equations (similar to those in the gravity case above) give the following results:

(1) Equivalent sources of  $S_3[A]$  are continuously distributed dipoles on the body surface  $C$  with a density

$$\sigma(M) = (R_{O'M})_v \mathbf{J}; \quad (\text{A14})$$

(2) Equivalent sources of  $S_0[A]$  are continuously distributed dipoles on  $C$  with a density

$$\sigma(M) = J_v \mathbf{R}_{O'M}, \quad (\text{A15})$$

where  $\mathbf{v}$  is the outward normal to the surface  $C$  at points  $M$ . The results obtained in the case (c) above are in accordance with (A14).

The physical interpretation of  $S[A]$ , as an anomalous field of equivalent sources, helps in formulating and implementing Euler inversions of gravity and magnetic anomalies using differential similarity transformations.

## Appendix B

### Geometrical transformations of similarity and homotopy

A similarity transformation in a 3D space with points given by the Cartesian coordinates  $x_1, x_2, x_3$  has the matrix equations (e.g. Gellert, Kastner and Neuber 1979),

$$\mathbf{x}' = \mathbf{A}\mathbf{x} + \mathbf{b}, \quad \mathbf{A}\mathbf{A}^T = t^2\mathbf{E}, \quad t > 0, \quad (\text{B1})$$

where  $\mathbf{x} = (x_1, x_2, x_3)^T$  is the column vector of a given point  $P$  and  $\mathbf{x}' = (x'_1, x'_2, x'_3)^T$  is the column vector of the resultant point  $P'$ ,  $\mathbf{b} = (b_1, b_2, b_3)^T$  is the column vector of a

given translation,  $(^T)$  is a sign of transposition,  $\mathbf{A}$  is the transformation matrix, given by

$$\mathbf{A} = \begin{pmatrix} a_{11} & a_{12} & a_{13} \\ a_{21} & a_{22} & a_{23} \\ a_{31} & a_{32} & a_{33} \end{pmatrix}, \quad \mathbf{E} \begin{pmatrix} 1 & 0 & 0 \\ 0 & 1 & 0 \\ 0 & 0 & 1 \end{pmatrix},$$

and  $t$  is the coefficient of similarity given as a positive real number. This transformation maps a straight line  $L$  on to a straight line  $L'$ , which may or may not be parallel to  $L$  depending on the coefficients of the matrix  $\mathbf{A}$ . The angle  $\alpha$  between two lines  $L_1$  and  $L_2$  is preserved between the corresponding lines  $L'_1$  and  $L'_2$ , i.e.  $\alpha' = \alpha$ . The ratio between two segments is also preserved. Two geometrical figures are similar to each other if a transformation (B1) between them can be composed with a regular matrix  $\mathbf{A}$ .

In particular, if the matrix coefficients  $a_{12} = a_{13} = a_{21} = a_{23} = a_{31} = a_{32} = 0$ , then (B1) takes the simple form

$$x'_i = tx_i + b_i, \quad i = 1, 2, 3, \quad t > 0. \quad (\text{B2})$$

In this case a straight line  $L$  maps on to a straight line  $L'$  parallel to  $L$ . A point, whose coordinates satisfy the equations  $x_i = tx_i + b_i$ , is an immovable point. This is a unique point  $C$  having the coordinates  $c_i = b_i/(1 - t)$ ,  $t \neq 1$ . Such a point  $C(c_1, c_2, c_3)$  is the central point of similarity. A similarity transformation (B2) can be performed in respect of a given centre  $C(c_1, c_2, c_3)$ , instead of a given translation vector  $\mathbf{b}$ , by the equations

$$x'_i = tx_i + (1 - t)c_i, \quad i = 1, 2, 3. \quad (\text{B3})$$

In a 2D space (a plane), the same equations are valid at  $i = 1, 2$ . Figure 1 illustrates the effect of (B3) on a source figure and on a line of observation points of a 2D anomalous field. Equations (9) correspond to the equations (B3).

A homotopic transformation has the equations (B3), where  $C(c_1, c_2, c_3)$  is the central point of homotopy and  $t$  is a coefficient, which may be given by a positive or by a negative real number. In the case of a central point  $C$  coinciding with the origin of the coordinates,

$$x'_i = tx_i, \quad i = 1, 2, 3, \quad t \neq 0 \quad (\text{B4})$$

are the respective simple equations of a homotopic transformation. If  $t > 0$ , then the homotopic transformation does not differ from the similar transformation (B3). If  $t < 0$ , then the geometrical figures shift in the opposite direction and their orientation alternates. These changes complicate the relationships between the original and transformed sources and their fields. The similarity transformation (B3), having by definition a positive coefficient, is more suitable for the search, formulation and implementation of inverse techniques based on Euler's homogeneity

## References

- Apostol T.M. 1957. *Mathematical Analysis*. Addison-Wesley Pub. Co.  
 Barongo J. 1984. Euler's differential equation and the interpretation of the magnetic point-pole and point-dipole source. *Geophysics* **49**, 1549-1553.

- Draper N.R. and Smith H. 1966. *Applied Regression Analysis*. John Wiley & Sons, Inc.
- Fairhead J.D. and Green C.M. 1994. Application of semi-automated interpretation methods in Western Siberia and Southern Sudan. 56th EAEG meeting, Vienna, Extended Abstracts, I037.
- Fishback W.J. 1964. *Projective and Euclidean Geometry*, 2nd edn. John Wiley & Sons, Inc.
- Gellert W., Kastner H. and Neuber S. 1979. *Lexikon der Mathematik*. VEB Bibliographisches Institut, Leipzig.
- Gill P.E., Murray W. and Wright M.H. 1981. *Practical Optimization*. Academic Press, Inc.
- Hood P. 1965. Gradient measurements in aeromagnetic surveying. *Geophysics* 30, 891–902.
- Leite L.W.B. and Leao J.W.D. 1985. Ridge regression applied to the inversion of two-dimensional magnetic anomalies. *Geophysics* 50, 1294–1306.
- Reid A.B., Allsop J.M., Granser H., Millet A.J. and Somerton I.W. 1990. Magnetic interpretation in three dimensions using Euler deconvolution. *Geophysics* 55, 80–91.
- Slack H.A., Lynch V.M. and Langan L. 1967. The geomagnetic gradiometer. *Geophysics* 32, 877–892.
- Solovev O.A. 1960. A method of magnetic interpretation using vertical and horizontal gradients of  $Z_a$ . Proceedings of the Institute of Geology and Geophysics, Siberian Academy of Sciences, 1, 15–22 (in Russian).
- Stavrev P. 1975. Variant transformations of anomalous field. *Comptes Rendus de l'Academie Bulgare des Sciences* 28, 2, 177–180 (in Bulgarian).
- Stavrev P. 1981. Similarity transformations of gravity and magnetic anomalies. *Bulgarian Geophysical Journal* VII (3), 95–106.
- Telford W.M., Geldart L.P. and Sheriff R.E. 1990. *Applied Geophysics*, 2nd edn. Cambridge University Press.
- Thompson D.T. 1982. EULDPH: A new technique for making computer-assisted depth estimates from magnetic data. *Geophysics* 47, 31–37.
- Zhaofang Zhu 1994. Interpretation of aeromagnetic data using 3D Euler deconvolution and 3D analytic signal in the Qinling orogenic belt, China. 56th EAEG meeting, Vienna, Extended Abstracts, P005.